BLOCK COPOLYMER VESICLES:

SELF-ASSEMBLED BEHAVIOR FOR USE IN BIOMIMICRY

A Thesis

by

JEFFERY SIMON GASPARD

Submitted to the Office of Graduate Studies of
Texas A&M University
in partial fulfillment of the requirements for the degree of

MASTER OF SCIENCE

December 2007

Major Subject: Chemical Engineering

BLOCK COPOLYMER VESICLES:

SELF-ASSEMBLED BEHAVIOR FOR USE IN BIOMIMICRY

A Thesis

by

JEFFERY SIMON GASPARD

Submitted to the Office of Graduate Studies of
Texas A&M University
in partial fulfillment of the requirements for the degree of

MASTER OF SCIENCE

Approved by:

Chair of Committee,	James Silas
Committee Members,	Mariah Hahn
	Melissa Grunlan
Head of Department,	Michael Pishko

December 2007

Major Subject: Chemical Engineering

ABSTRACT

Block Copolymer Vesicles:

Self-Assembled Behavior for Use in Biomimicry.

(December 2007)

Jeffery Simon Gaspard, B.S., Texas A&M University

Chair of Advisory Committee: Dr. James Silas

The objective of this research is to investigate synthetic and polypeptide block copolymers, the structures they form, their response to various stimuli in solution and their capabilities for use in biomimicry. The self-assembled structures of both polymers will be used as a basis for the templating of hydrogels materials, both in the interior and on the surface of the vesicles. The resulting particles will be designed to show the structural and mechanical properties of living cells.

The synthetic block copolymers are a polyethylene glycol and polybutadiene (PEO-*b*-PBd) copolymer and the polypeptide block copolymers are Lysine and Glysine (K-*b*-G) copolymers. Investigation of the structures synthetic block copolymers will focus on whether the polymer can form vesicles, how small of a vesicle structure can be made, and the formation of internal polymer networks. Subsequent investigations will look at the needed steps for biomimicry, using the synthetic block copolymers as a starting point and transitioning to a polypeptide block copolymer.

The Lysine-Glysine copolymers are a new system of materials that form fluid vesicle structures. Therefore, we must characterize its assembly behavior and investigate

how it responds to solution conditions, before we investigate how to make a cellular mimic from it. The size and mechanical behavior of the K-G vesicles will be measured to compare and contrast with the synthetic systems.

The goals for creating a biomimic include a hollow sphere structure with a fluid bilayer, a vesicle that has controllable mechanical properties, and a vesicle with controllable surface chemistry. Overall, these experiments were a success; we showed that we can effectively control the size of vesicles created, the material properties of the vesicles, as well as the surface chemistry of the vesicles. Investigations into a novel polypeptide block copolymer were conducted and the block copolymer showed the ability to create vesicles that are responsive to changing salt and pH concentrations.

ACKNOWLEDGEMENTS

I would like to thank Dr. Silas for his support and guidance through all the research and experimentation. He is a great educator and a constant source of inspiration.

I would also like to thank the members of my committee, Dr. Mariah Hahn and Dr. Melissa Grunlan. Without these two professors, I would not have been able to finish this work and experimentation.

I would also like to thank the members of my research group, Karym Kinnibrugh, Clemente Contreas, and Winnie Chang. I would also like to thank members of other research groups that helped me throughout my research, Shannon Eichmann of Dr. Michael Bevan's group, Allen Bulick and Dany Munoz of Dr. Mariah Hahn's group and Dr. Jeng Shiung of Dr. Dan Shantz's group. Without these individuals, this research could not have been done.

TABLE OF CONTENTS

Page

Page

LIST OF FIGURES

Page

Page

LIST OF TABLES

Page

I. INTRODUCTION

1.1 Overview

Block copolymers bridge several research areas including self-assembled materials and polymer physics. Amphiphilic di-block copolymers, copolymers with one hydrophobic and one hydrophilic block, are designed to form self-assembled structures in water, including vesicles and micelles[1, 2]. The use of self-assembled materials spans many different fields of scientific research, but our primary motivation for this research is biomimicry.

Several studies[1, 3-9] have been directed at using polypeptides as one or all of the blocks in a copolymer. Polypeptide synthesis has been fueled by the interest of making a natural polymer that would have some ability to interact with biological systems, such as the human body[1]. The two main categories of block copolymers utilizing polypeptides are synthetic-polypeptide copolymers and all polypeptide copolymers.

The constituent blocks of amphiphilic block copolymers can be made from amino acids or synthetic components. Since the investigation into creating vesicles using synthetic block copolymers is well established, these polymers will be used as a basis for testing and experimenting with the attributes needed for a biomimic. One goal will be to incorporate the use of polypeptide block copolymers to make vesicles for use in a biomimic, rather than relying on the synthetic block copolymers. Since the self-

---

This thesis follows the style of *Science*.

assembly properties of polypeptide block copolymers are not as well understood as the self-assembly properties of synthetic block copolymers, polypeptides must be studied more carefully before they can be incorporated into biomimetic particles.

The main requirements we wish to achieve in a cellular mimic are a hollow sphere, fluid bilayer, adjustable or controllable surface chemistry, responsive particles to solution conditions, and controllable mechanical properties. This thesis will focus on particles responsive to solution conditions, controllable surface chemistry and controllable mechanical properties.

1.1.1 Biomimicry

While there are different reasons for wanting to create a biomimic, this research focuses on two. The first reason is a purely research goal; create an artificial membrane or membrane system to test biological functions. Another reason for developing a mimic is for drug delivery or other medical therapies in which compounds of interest can not be solubilized easily in aqueous conditions.

In order to have a true biomimic, we need to mimic the basic structure and features of a living cell. Some of the traits or components living cells possess are a fluid bilayer membrane that encloses a spherical volume, an easily modified surface, characteristic mechanical properties, and a responsive nature to surrounding conditions.

The first component of our biomimic is a synthetic membrane analogous to a natural cell membrane. Making a bilayer membrane is easily achieved with the use of amphiphilic block copolymers that create vesicles. These copolymers self-assemble into

a vesicular macrostructure in aqueous conditions, and are discussed in more detail in the next two major sections.

The second component of our biomimic is an easily modified surface chemistry. A tailored surface chemistry allows the mimic to be a "smart" creation, interacting with the solution and conditions present in a predesigned way. If the vesicle contains an easily reacted site or retains the ability to add specific components after the vesicle has been formed, the biomimic can selectively interact with its surroundings through modifications of the reactive sites on the vesicle. This is best achieved by making some of the copolymer chains in the vesicle's bilayer reactive. Two methods are outlined in subsequent sections.

A third component for biomimicry is controllable mechanical properties. Using the synthetic copolymer system, encapsulation of various polymer networks will be used to tailor material properties similar to natural systems, such as the cytoskeleton, the cytoplasm and the actin network. Tailoring the specific material characteristics will depend on the type of internal network that will be modeled.

The remaining components of the biomimic are fluid bilayers and responsive particles. Both of these traits are incorporated into the novel polypeptide block copolymer investigated in these experiments. The polymer is a polyelectrolyte, which will allow the polymer to change due to salt or pH conditions. The polymer also possesses a hydrophobic section that does not contain any reactive sites nor does it change its conformation in solution due to changing conditions.

The two general types of block copolymers investigated in this research are a synthetic block copolymer of polyethylene oxide-block-polybutadiene (E_mBd_n) and a

polypeptide block copolymer, made from polylysine-block-polyglysine (K_mG_n), where *m* and *n* denote the number of units in each block. For the synthetic block copolymer, the hydrophobic section is butadiene; while for the polypeptide block copolymer the hydrophobic section of polymer is glysine. Both hydrophobic blocks form random coils in solution. This feature allows both synthetic and polypeptide vesicles to maintain a fluid hydrophobic region, rather than a crystalline or glassy bilayer. Fluid bilayers are most responsive to changes in solution conditions and give rise to thermodynamically stable bilayer phases, rather than kinetically trapped structures. Each of these copolymers will be discussed in the next two major sections.

1.2 Synthetic Block Copolymers

Synthetic analogues of a natural membranes system is an area that has garnered much interest[10-15]. The result of others' research is a fluid bilayer sphere, similar to a cell membrane, called a vesicle. Whether from a small molecule lipid or a block copolymer, vesicles have been instrumental in understanding the chemistry and physics of the cell membrane. Block copolymer vesicles have the same advantages as lipid vesicles, but with greater stability and ease of use[12, 14, 16]. Studies[10, 11, 17] show how chain length and chemistry of the block copolymers used for the bilayer will affect the bending modulus, the rigidity, the elasticity, the stability, and the ease of assembling in solution[10, 11, 18-20]. Much of the formational procedures on how to make vesicles are adapted from Hammer and the lipid vesicle literature.

1.2.1 Surface Modification

The second component of our mimic is surface modification for responsive particles. The ultimate goal of this area would be to have a particle with many different moieties incorporated onto the surface, similar to a real cell. Several studies[17, 21-24] have shown simple procedures in which the ends of the block copolymers can be modified or functionalized to include easily spliced leaving groups, such as tresyl chloride. Tresylated polymer can be incorporated into the bilayer and later reacted in order to have various functional groups on the surface of a vesicle. The drawback to this system is that the overall conversions of the reactions are low, whether it is the reaction of the end groups or the creation of the tresylated polymer.

A newer approach to this problem is looked at by our research group. In our procedure, the hydroxyl ends of the polymer are converted into a carboxylic acid group, which allows for peptide linkage chemistry of any amine functional group.

1.2.2 Internal Structure

The third component of our cellular mimic is the formation of an internal structure. The purpose is to create an analogue to the cell's cytoskeleton within the bilayer of the block copolymer vesicle. By coupling the bilayer to an internal structure, the vesicle becomes more robust, being able to withstand solution conditions that would mechanically rupture the vesicle bilayer alone. Also, this gives us the ability to attach compounds of interest to the internal network that can span the membrane and reach outward to the solution. If this is achieved, the internal network and not the membrane

supports the stresses and shear of attachment, much like cell-surface attachments, and allows the mimic to more accurately model cellular mechanics. One example is cell adhesion studies[17, 21, 22, 24]. These studies relied on the hydrophobic region to hold on the block copolymer that was chemically linked to the ligand, instead of trying to have a trans-membrane member that can link with the ligand and act as an extension of the internal polymer network. Forces applied to the ligand would be transferred down the extension and into the mass of polymer, similar to the foundation of a building. An approach for creating an internal polymer network is that of templating. An example is shown in Figure I-1.

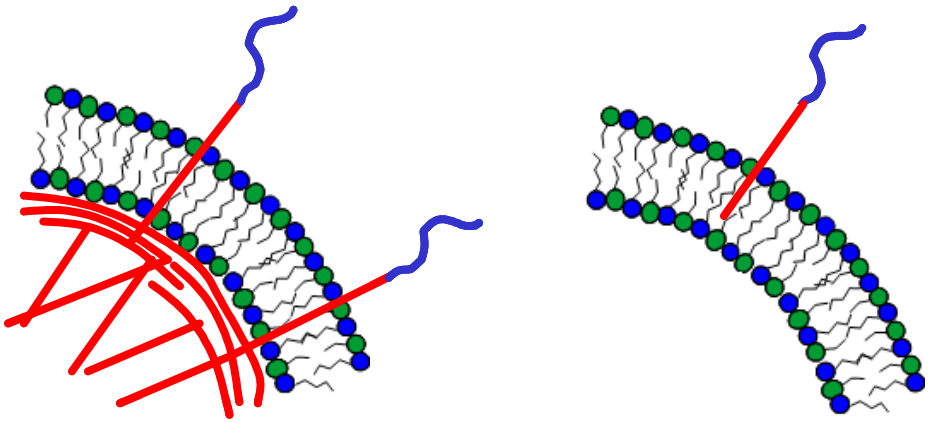

Figure I-1: Ligands linked to extensions from an internal polymer network. The figure on the left is a representation of an extension of the interior polymer network and a functional group attached to the extension. If the ligand undergoes stresses, the force is transferred to the internal network and structure, not just the membrane. The figure on the right is how current methods attach functional groups to the membrane. The ligand is held in the hydrophobic section of the membrane. Stresses from the ligand are applied to the membrane and if enough force is applied, the vesicle membrane will rupture, causing the destruction of the vesicle.

1.2.2.1 Templating

Templating is a process that builds a temporary structure so that the more permanent, desired structure can be built with increased ease. Much of the interest in the idea of templating builds off the ability to create new, more complex structures by templating the structure of an organized material in solutions. A biological example of this phenomenon is biomineralization of structures on the cellular level. Being able to produce an ordered structure from a previously self-assembled structure is of great interest in material and catalyst research. By looking at the way the template is assembled in solution, we can build better templates, ones that can cross multiple length scales. In building a better template, we might also be able to include complex features into the structure that would then be transferred to the superstructure built off of the template, such as pores or internal supports.

This research focuses on building a better template, rather than the end structure. Much of the work done so far deals with creating a more complex template that leads to a more complex structure. For this proposal, we will be looking at the template itself and creating a simple structure inside the template.

Previous work from which this research draws deals with three main areas: 1) templating of structures for organized media, 2) robust templates, and 3) encapsulation. The first area, templating of structures for organized media looks at organized gels using a copolymer or surfactant.

1.2.2.1.1 Organized Media

As shown by Kaler[25] and others [26-34], creating organized gels or structures from copolymers is easily done. Most of the techniques discussed in the papers deal with using the surfactant or copolymer to solubilize the superstructure material. Upon polymerization of the superstructure material, the vesicles or template structures are destroyed, due to mechanical stresses or with added solvent, and the copolymers or surfactants are removed, leaving behind the superstructure.

1.2.2.1.2 Colloidal Interest

Templating using a copolymers or surfactants system for colloidal interests, in the form of small solid spheres of polymer, has been successful[34-38]. Colloidal interest experiments typically focus not on making a superstructure, but creating a uniform distribution and reproducible particle using surfactant/copolymer. The area of interest deals mostly with latexes, from paints to biological interests. Gin [39] and Kaler [40] both report on using surfactants for microemulsions. Forming microemulsions differ from organized media experiments because the surfactant rearranges and stabilizes the particles as the polymerization takes place. These techniques result in particles less than 100 nm in size, whereas the organized media experiments create particles up to several microns in size.

1.2.2.1.3 Robust Template

For some copolymer or surfactant systems, a narrow range of operating temperatures, solution conditions and solvent concentrations exist. One approach for a robust template is a polymerized shell; whereas the copolymer or surfactant is chemically linked to each other, making the current shape permanent. This can be achieved several different ways; having a double bond in the copolymer chain, introducing an agent that will bond with the hydrophobic section of the copolymer or surfactant system, or an agent that will interact with the hydrophilic section of either the copolymer or surfactant system. The advantage of polymerizing the shell is the vesicle becomes impervious to mild and moderate changes in solutions and conditions. In Discher [16], polymerized vesicles were subjugated to chloroform which, under normal circumstances, would redissolve the polymer monomerically and destroy the vesicle. But being polymerized, the shell could not rearrange or redissolve, thus keeping the vesicle intact. Vesicles were also subjugated to being pulled out of solution, air dried, and then placed back inside of solution. The particles were able to maintain their shell and return to normal solution behavior once placed back into solution.

Using a surfactant system and swelling the hydrophobic region to create a vesicle shell is done by Jung[41] and Meier[42]. These two similar systems create vesicles with a surfactant, and then dissolve a hydrophobic monomer, either heptadiene or a methacrylate, into the solution, forcing the monomer to reside inside the hydrophobic layer. The monomer is then polymerized, and the surfactant removed. The resulting shell is stable and considered a two dimensional polymer network.

Another motivation to create particles that can withstand drying out the vesicle solution and resuspending the sample in another solvent. Kaler[43, 44] provides two examples of creating vesicles with polymerized shells and drying out the solution. One application for this is creating ordered hard material from vesicle structures. Creating hard, ordered materials, such as silica synthesis, require solvents and conditions in which the vesicles would be redissolved or mechanically destroyed. Creating vesicles in an aqueous environment and then being able to put them into another solution is desirable.

1.2.3 Encapsulation

Encapsulating chemicals by creating vesicles is interesting because vesicles contain a separate aqueous center that is only reachable through the vesicle membrane. The separate aqueous volume allows the vesicles to sequester a compound of interest, such as monomer. Encapsulating a monomer inside a vesicle is the pathway in which we will attempt to tailor the mechanical properties for the biomimic. By encapsulating monomer on the inside of a vesicle, we can create a microgel, or if we encapsulate two reactive chemicals, we can create a nanoreactor.

Graff[45] presents a complex nanoreactor system. Here, they are able to create a vesicle structure with a large protein built into the bilayer. By swelling the bilayer with a methacrylate and then polymerizing the hydrophobic section, the vesicle still maintains some of the mobility the shell possessed before being polymerized. Proteins were incorporated into the shell of the vesicle that selectively allowed the passage of small molecules, in particular ampicillin. The protein in the bilayer allows ampicillin to enter

the vesicle, wherein it is attacked by an encapsulated enzyme, and then the product is expelled. The rate of enzymatic activity is monitored by an iodine stain, easily telling about the kinetics of the system.

Another encapsulation system of interest is making a temperature dependent particle, similar to Jesorka[46]. They created giant unilamellar vesicles (GUVs) and then inject into the GUV various solutions of N-isopropyl-acrylamide (NIPAM) into the interior of the vesicles. Using light microscopy, they observe the changes in the vesicle as they raise and lower the temperature above the lower critical solution temperature (LCST), for NIPAM, approximately 32^{o}C. The vesicle undergoes a phase change, having the NIPAM precipitate out of solution as the temperature rises, and then having the NIPAM come back into solution as the temperature cools.

By integrating a combination of these cited techniques and ideas, we hope to achieve our research goal in creating a complex particle that is capable of biomimicry.

1.3 Polypeptide Block Copolymers

1.3.1 Synthetic-Polypeptide Hybrids

Synthetic-polypeptide block copolymers are polymers in which one of the blocks is a synthetic polymer, usually a long hydrocarbon chain. Di- and tri-block copolymers have been used to create micelles for either gene therapy or other medical treatments[5-7]. Kataoka et al. show some success in creating micelles in solution that have the ability to assembly into approximated 100 nm structures.

Other groups[3, 4, 8, 9] have focused on block copolymers that make vesicles instead of micelles. Deming[9] shows how to make functionalized peptides that will also form

secondary structures in solution. The idea of having the block copolymer possess the ability to form a secondary structure is interesting, as it could provides a pathway to force the polymer into or out of solution. Lecommandoux[3, 4, 8] has created several polymers that are pH responsive, causing the secondary structure to change from a random coil at pH 7 to an alpha helix at pH 11. Their polymer is a synthetic-polypeptide hybrid, with the polypeptide being the block that changes its conformation. The novel polypeptide block copolymer developed by Dr. Shantz is completely amino acid based, but retains the same characteristics as Lecommandoux.

1.3.2 Polypeptide-Polypeptide Copolymers

The third variation of block copolymers are those made completely of amino acids. These polymers have similar issues as the synthetic-polypeptide polymers, but their chemical, physical and solution behavior are more complicated in that both peptide chains may fold. If one block is capable of forming a secondary structure in aqueous solutions, that block might alter the delicate balance of forces controlling self-assembly and cause the polymer to precipitate out of solution. Multi-peptide block copolymers have different sections of peptides that could potentially fold at different solution conditions thus yielding multiple triggers for precipitation.

Table I-1: List of available polypeptide block copolymers from Dr. Shantz lab, TAMU.

2:1 K:G ratio	4:1 K:G ratio	Triblocks
$K_{110}G_{55}$	$K_{120}G_{30}$	$K_{48}G_{12}$ K_{48}
$K_{320}G_{160}$	$K_{200}G_{50}$	$K_{120}G_{30}$ K_{120}
$K_{400}G_{200}$	$K_{345}G_{85}$	$K_{160}G_{40}$ K_{160}
		$K_{110}G_{55}$ K_{110}

Peptide block copolymer synthesis is a complicated multi-step procedure during which failure can occur before the final polymerization step. Deming[47] outlines the steps needed to create high molecular weight block copolymers. Dr. Shantz and Dr. Jeng Shiung have provided access to the polypeptide block copolymers listed in Table I-1.

There have been a few attempts to determine the assembly behavior of these types of polymers in solution, as well as polymer behavior during changing solutions conditions[48, 49]. These attempts have been mostly centered on cryogenic tunneling electron microscopy (cryo-TEM) and TEM. The limitations of these approaches are that cryo-TEM is difficult to obtain useful results, since freezing the solutions can alter the structures formed in solution if the freezing process is done incorrectly. TEM works well for imaging solid materials, but the particles of interest are solution based. By drying out the polymer, the structures that are formed during the drying process are different that those created in solution. The dried structures are that of polymer aggregation, not self-assembly.

There have been several other copolymers developed by other groups[50-52], such as poly(γ-benzyl L-glutamate), poly(L-lysine)- b-poly(L-leucine), and poly(L-lysine)-b-poly(L-leucine and L-valine). The latter polymer has two parts, a homopolymer block of lysine and a random block of leucine and valine as the other block. These polymers were investigated due to their ability to respond to solution changes, usually pH, as well as their desire to use the polymers to template superstructures or take advantage of the ordering of the blocks in solution. One problem with the previous studies is that the experiments are carried out in deionized water, after dissolving the polymer in a solvent. This method is an acceptable method to create vesicles, regardless of polymer type, but

since the polypeptide polymers are polyelectrolytes, placing the polymer in a solution without screening ions can cause the polypeptide polymer to adopt a highly strained configuration. To obtain fluid bilayers, we want to moderate the repulsions between the charged blocks on the polymer. By including adequate amounts of salt, one should be able to offset any issues that would arise from using deionized water. Also, the total molecular weights for these copolymers are low, as compared to the copolymer used in our experiments.

1.3.3 Responsive Particles

Responsive particles have been a subject of research for many years. Some recent work has focused having vesicles or micelles to respond due to changing pH or ion concentration[53, 54]. These studies examined getting a block copolymer to invert in solution to controlling size of self assembled structures, rather than the responsiveness of an aggregation of polymer in solution.

1.3.4 Novel Polypeptide Block Copolymers

The polymer of interest is a block polypeptide copolymer of Lysine and Glysine. Glysine was chosen because it is hydrophobic and a random coil. Lysine is a hydrophilic amino acid that has been used in many other experiments plus it is capable of changing shape in solutions with a pH greater than 11. For pH >11, polylysine will change from a random coil at neutral pH to an alpha helix in basic conditions. This block copolymer

should be pH responsive and form a self assembled, thermodynamically stable structure in solution, rather than a kinetically trapped vesicle.

There are several reports of amphiphilic block copolymers that form vesicles upon rapid dilution into water[47, 49, 52, 55-58], but the hydrophobic block is polystyrene, phenylalanine, or another block that is glassy or crystalline at the final solution conditions. These vesicles are not in dynamic equilibrium with monomers in solution, and therefore cannot be viewed as thermodynamic complex fluids – the energy to remove or insert a molecule is much higher than k_BT. The thermodynamic aspect of the vesicles found in these studies is that the bilayer is the dynamic and thermodynamically stable phase. Any changes to the system conditions, such as pH change, extrusion, sonication, dialysis or vortexing, may the vesicles to rupture, forcing the polymer to spontaneously reform into a bilayer. The size may change due to experimental procedures, but the bilayer will continue to be the most thermodynamically stable point.

II. METHODS

2.1 Naming Convention

The naming conventions for the samples are as follows: polymer type, followed by the percentage by weight and the polymer encapsulated and if a fluorescent dye was added. If acrylamide was added to the sample, a –XX is added, where the XX is the crosslink ratio, the number of monomer units to crosslinkers. If no number is indicated with acrylamide polymer, it is the 19:1 ratio monomer. A sample name would be $E_{20}Bd_{33}$ 10% AM-F, indicating $E_{20}Bd_{33}$ polymer with 10% acrylamide and FITC encapsulated on the inside. $E_{20}Bd_{33}$ 10% AM-38 would be $E_{20}Bd_{33}$ polymer with 10% acrylamide polymer with the 38:1 monomer to crosslink ratio.

2.2 Vesicle Formation

Table II-1: Listing of the synthetic block copolymers used in various experiments.

Di-block copolymer	Total MW (g/mol)	Blocks of PEO	Blocks of PBd
$E_{20}Bd_{33}$	2700	20	33
$E_{89}Bd_{120}$	10400	89	120
$E_{30}Bd_{46}$	3800	30	46

To make vesicles, polymers $K_{200}G_{50}$, $E_{20}Bd_{33}$, $E_{30}Bd_{46}$ or $E_{89}Bd_{120}$, shown on Table II-1, were used. A stock solution of a polymer was made to a concentration of 5 mg/mL. The solvent for the stock solution is methanol for the polypeptide polymer, chloroform or dichloromethane for the synthetic block copolymers. 50 μL of polymer

solution were aliquoted out into a vial to form a polymer film. An additional 400 μL of solvent was added to ensure an even film layer at the bottom. The vial was then placed inside of the vacuum oven and left overnight. Once the film was dried, a rehydrating solution was prepared. This solution is primarily sucrose, 300 mOs (0.3 M). If more than one sample is made, the rehydrating solution was made in an additional vial, then aliquoted out in 2 mL quantities to the individual samples.

Once the rehydrating solution has been added, the vesicles are placed overnight in the oven at 60^{o}C. The vesicle solution is then removed and cooled, either by placing the vial in the refrigerator or placing the vial on the lab bench for a short while.

2.3 Alternate Vesicle Formation

Polypeptide block copolymer can be placed into a vial containing a rehydrating solution and form vesicles without having to first make a film. This procedure involves making the correct rehydrating solution, usually a 300 mOs (0.3 M) sucrose solution, and placed the same amount of polymer, around 250 μg, directly into the vial. The sample is then vigorously vortexed for several minutes to make sure the polymer is distributed throughout the vial. This will ensure the solvent is displaced, causing the polymer to rearrange in solution and form vesicles. The vesicles formed this way are generally smaller and not as efficient, with more aggregated polymer observable in the samples as with the normal vesicle creation method.

2.4 Polymer Encapsulation

Encapsulating monomer on the inside of the vesicle requires a monomer to be placed in the rehydrating solution, from 5-40%, by weight. See Table II-2 for the amounts of monomer in the specific type of polymer encapsulated vesicle. Along with encapsulating monomer, a fluorescent dye is usually added to the monomer, giving the particles a single color. In most cases, FITC is the fluorophore that is added to the monomer.

Table II-2: Various polymer recipes used in the encapsulation experiments. These recipes are for 2 mL of rehydrating solution.

Type*	AM (μL)	NIPAM** (μL)	PHEMA (μL)	X-Link*** (μL)	Sucrose (μL)
AM 5%	250	0	0	1.125	1750
AM 10%	500	0	0	2.5	1500
NIPAM 5%	8.4	1000	0	0.42	1000
NIPAM 10%[1]	16.8	2000	0	0.84	0
PHEMA 5%	1.125	37.5	80	0.05625	1881
PHEMA 10%	2.25	75	160	0.1125	1763

[1] – For this solution, the NIPAM is dissolved in sucrose, instead of DI water.
* - This is solution amounts for each 2 mL vial
** - NIPAM is a 10% stock solution made in the laboratory for ease in aliquoting.
*** - The crosslinker is included in the acrylamide

2.5 Linked Fluorescent Bilayers

For dual color vesicles, the same vesicle formation procedure was followed, except for the film creation step, 10% acid polymer, by weight of initial polymer, was added to the film. Five μL of acid polymer was added, with 45 μL of E_{89}-Bd_{120} polymer added for the film. The acid polymer was prepared beforehand and supplied by Karym Kinnibrugh, from Dr. Silas Research group. The additional 400 μL of chloroform was

added to ensure the even film on the bottom of the vial. After the vesicles have been formed and polymerized, an EDC/NHS reaction would attach a coumarin-based dye to the ends of the acid polymer. This reaction was performed by Karym Kinnibrugh.

The peptide linkage reaction is well known and utilizes EDC and NHS[59-62]. The procedure involves taking a prepared sample, in this case a vesicles solution of E_{89}-Bd_{120} 10% AM-F with 10% acid polymer, and reducing the solution to a pH of 6. The next step is to add in a 5 times molar excess solution of EDC and a 3 times molar excess solution of NHS. The solution is allowed to react for 15 minutes and then the pH is raised back to 7-7.5. The coumarin-based dye is added to the reaction, and since it has a primary amine, it is linked to the acid polymer in the vesicle bilayer. Several additions of EDC and NHS are added over several hours to increase the yield of the reaction of coumarin-based dye to the acid polymer. Once the reaction has finished, the sample is placed in a dialysis cassette and cleaned out. The procedure for dialysis is explained in section 2.8.

2.6 Fluorescent Bilayers

In the case of some samples, a fluorophore, such as Nile Red or C-9 Acridine Orange, is added to the film polymer solution so that the fluorescent marker is even distributed into the bilayer. The stock solution for the fluorescent marker is made with the same solvent that the polymer is dissolved in. The fluorophore is added to a small centrifuge vial, along with the polymer solution and vortexed gently to ensure even distribution. The solution is then taken and placed in a sample vial and extra solvent is added, following the normal procedure to make vesicles.

A stock solution of Nile Red was made with a final concentration of 0.1 mg/mL. Nile Red was added after the polypeptide block copolymer had been aliquoted into a vial. A ratio of 4:1 polypeptide to Nile Red was added to the vial and then an additional 400 μL of MeOH was added to the whole solution to create a more uniform film. The final steps are exactly the same as the normal vesicle formation steps.

2.7 Extruding Vesicles

In order to create a more monodisperse or a specific size sample of vesicles, the solution of vesicles can be extruded. Extruding a sample is forcing the solution through a filter with a predetermined pore size, making the vesicles break open in order to pass through the filter. The pore size of the filter will ultimately determine the size of the vesicles that are created.

To extrude a sample, after the vial is taken out of the oven, the chamber is prepared. This involves rinsing the syringes and filters in aqueous solution so that the osmotic pressure of the surfaces is equal to that of the bulk solution, then loading the sample and pushing the sample through the filter the required number of times. All extrusions are done with an odd number of passes to make sure the samples stay clean. Once the sample has been extruded, dialysis and polymerization follows.

Before a sample is extruded, it might be necessary to run the sample through several freeze/thaw cycles. Putting samples through a freeze/thaw cycle causes vesicles to break apart due to the shearing forces during rapid cooling. By repeating the

freeze/thaw steps several times, larger vesicles can be broken into smaller vesicles before extrusion.

A Freeze/thaw cycle involves taking the vesicle sample and placing the entire vial in a bath of liquid nitrogen. After several minutes, the whole sample is frozen. With care, the sample is removed, and placed on a metal shelf for several minutes. This gives the glass sample vial time warm up so that the immersion into tepid water does not cause the glass to break. The sample is kept under tepid water until the sample has completely melted. Once the solution has melted, the sample is placed back into the liquid nitrogen. This is repeated several times, usually 5, and after the final warming up of the solution, the sample is extruded.

The extruding device consists of two gas-tight syringes, 1 mL each, a Teflon chamber and a stainless steel jacket. Each syringe inserts into half of the overall Teflon chamber. The two halves have between them four filter supports and one filter. Two supports are placed on either side of the filter and the Teflon blocks are compressed together. The Teflon and filter system is placed into a stainless steel jacket that is screwed together to hold the filter and Teflon tightly. The syringes are then inserted into holes on opposite sides of the stainless steel jacket.

The filter system needs to be wetted and brought up to the correct osmotic pressure to make sure that the vesicles are not destroyed during extrusion. Several passes are made with a syringe full of DI water, followed by several sets of several passes of iso-osmotic phosphate buffer solution (PBS). Once the syringe and Teflon chamber are wetted, the sample is drawn into one syringe and extruded the request number of passes.

2.8 Dialysis

Dialysis is done to remove the monomer or other chemicals that did not get encapsulated inside the vesicles. The first step in performing dialysis is done by preparing a PBS solutions that is slightly higher in osmotic pressure than the sucrose solution, usually 310 mOs (0.31 M). A dialysis cassette is prepared by soaking it in the PBS for 5-10 minutes, then injecting the sample into the cassette. The dialysis cassette is placed in the beaker of PBS and stirred gently for 3-4 hours.

Once the time has passed, the samples are removed and placed in a new vial. Before the samples are removed, a small amount of higher osmotic pressure PBS is added to the sample inside the cassette. This causes a flux of solution into the cassette and improves the recovery yield of vesicles.

2.9 Dilution Approach to Cleaning

If the block copolymer can not contain the monomer inside the vesicle or dialysis would destroy the vesicles before the monomer could be polymerized, a dilution approach was used to polymerize the monomer. The sample is prepared following the normal vesicle creation technique. Once the sample is removed from the oven, a larger quantity of rehydrating solution was prepared. The new solution has the same osmotic pressure as the rehydrating solution, but without the monomer. The reason for making a solution with the same osmotic pressure is that the overall osmotic pressure difference on the vesicles needs to stay as close to zero as possible. Once the new solution is prepared, the sample is added to the larger volume solution. This is usually done in ratios of 10,

such as 1:9 sample to large volume. By adding the sample to the large volume of aqueous solution, the bulk exterior monomer concentration will fall below the minimum gelling value so that when polymerization occurs, the sample stays liquid. The sample is now polymerized using the ammonium persulfate/TEMED (APS/TEMED) solution. The sample is then centrifuged in which excess solution is drawn off and the vials are consolidated to bring the sample back to its original volume.

2.10 Polymerization of Monomer

Once the sample is removed from the oven and cleaned using the dialysis or the dilution approach, it is polymerized immediately. 120 μL of APS and 30 μL of TEMED are added to initiate the reaction. This reaction takes about 1-3 hours and the solution is usually vortexed to ensure even distribution of the initiators. The reaction method is a free radical initiation; the TEMED breaks apart the APS and forms a single radical for each chemical pair.

If the vesicles are to have just a polymerized shell, once the sample is removed from the oven, the same amount of APS and TEMED are added and allowed to react. The reaction takes about the same amount of time, 1-3 hours.

If the APS/TEMED system will not polymerize the solution fast enough, a light induced initiator is used. This solution is composed of N-vinyl pyrrolidone (NVP), 1 mL, and 2-Dimethoxy 2 phenylacetophenone (acetophenone), 300 mg. The acetophenone is a radical producer and initiates reactions in the same manner as the APS/TEMED system.

The photoinitiator is added to the sample and then the sample is placed under a UV lamp (250 nm). After a few minutes the sample is fully polymerized.

A final initiator system for the polymerization of monomer is that of VA-44 (2,2'-Azobis[2-(2-imidazolin-2-yl)propane] Dihydrochloride). This initiator is also a free radical initiator, but relies on the temperature to activate the compound; once the sample temperature rises above 44^{o}C, the initiator is activated.

2.11 Lipid Labeling

For some fluorescent vesicles, a fluorescently labeled lipid is added after the vesicles have been formed. For this, a small part of the sample is placed in a centrifuge vial, along with the lipid labeler. The solution is then vortexed vigorously for several minutes to get the lipid labeler evenly distributed in the vesicle's hydrophobic region.

In making fluorescently labeled vesicles with Acridine Orange, 3,3′-Dioctadecyloxacarbocyanine perchlorate (DiO), or 1,1'-dioctadecyl-3,3,3'3'-tetramethylindocarbocyanine perchlorate (DiL), vesicles are first made using the normal vesicle formation procedure. Since the fluorophore does not dissolve into aqueous solutions, methanol is added to dissolve the fluorophore so in order to be added to the sample, in a ratio of 500:1, block copolymer to dye. This ratio was added to make sure that the amount of methanol being added to the solution did not disrupt the vesicles.

2.12 Confocal Imaging

A three-sixteenth inch thick square rubber gasket with a hole cut of the center is placed on top of a 22x50 mm glass cover slip. A small amount, 30-50 μL, of the sample solution is added to the center. Slightly higher osmotic solution, 300-310 mOs, is added to the rest of the cavity, 120-150 μL. The sample is then placed on the confocal microscope and imaged using the 63x oil objective lens that has an NA of 1.25. Pictures are taken at a resolution of 1024x1024, at a refresh rate of 400 Hz, a pinhole size of 100 μm, and a voltage of 700 V for the photomultiplier tube (PMT).

2.13 Light Scattering Measurements

For testing the samples using a laser light scattering technique, the samples are made using the same formation technique, with the exception that everything is filtered to remove contaminates. A 0.22 μm syringe-tip filter is used for all liquids, from the methanol used to ensure an even film, to the sucrose rehydrating solution, to the a final filtration if the samples have been extruded, in order to remove bacteria, dust and other small particles not of interest.

For Dynamic Light Scattering (DLS) testing, the sample is added into the cuvette, about 800-1000 μL. Clean PBS is added to fill the vial up to about 3 mL. Part of the solution is then aspirated into a clean Pasteur pipette and shot back into the cuvette. This is repeated several times to mix the sample without introducing any air bubbles. The sample is then capped and placed in the machine for testing.

The machine, a Brookhaven Instruments ZetaPals DLS, is a self-contained light scattering machine. Testing parameters are controlled using the software, including time delays, solution conditions and testing time. The laser used is a HeNe, with an emission of 633 nm.

For Static Light Scattering (SLS) measurements, the sample basic idea persists. About 600-1000 μL of sample is withdrawn from the sample vial and placed in the glass test tube. Clean PBS solution is added to fill the test tube about three quarters full. The tube is either capped and vortexed gently to avoid air bubble formation or a clean Pasteur pipette is used to aspirate and shoot the solution to mix it up. The test tube is then inserted into the Goniometer for measurements.

The Goniometer is a Brookhaven Instruments Corporation machine as well. The system utilizes a Melles Griot HeNe laser that runs at 633 nm, with a maximum power output of 75 mW. For the testing trials, a sweep of 10^{o} to 155^{o} was used, at 5^{o} intervals.

2.13.1 Dynamic Light Scattering

Dynamic light scattering uses a time-correlation of the photoelectron count to obtain a size distribution of particles in solution. The general form of the equation is[6]

$$g^{(2)}(\tau) = 1 + \beta\left|g^{(1)}(\tau)\right|^2 = 1 + \beta e^{(-2\bar{\Gamma}\tau)} \qquad \text{(II.1)}$$

where

$g^{(2)}(\tau) =$ Normalized second order correlation function

$\beta =$ Parameter of the optical system, constant

$g^{(1)}(\tau)$ = Normalized first order correlation function

τ = Delay time

$\overline{\Gamma}$ = Average characteristic line width

$g^{(1)}(\tau)$ can be expressed by the following equation.

$$g^{(1)}(\tau) = \int G(\Gamma) e^{(-\Gamma\tau)} d\Gamma \tag{II.2}$$

where

$G(\Gamma)$ = Distribution function of Γ

The analysis of the autocorrelation functions used the method of cumulants, where

$$g^{(1)}(\tau) = \exp\left[-\Gamma\tau + \left(\frac{\mu_2}{2}\right)\tau^2 - \left(\frac{\mu_3}{3!}\right)\tau^3 + \ldots \right] \tag{II.3}$$

yields the average line $\overline{\Gamma}$ and a variance or polydispersity index of $\frac{\mu_2}{\overline{\Gamma}^2}$. This approach, the cumulant approach, gives us the z-averaged diffusion coefficient, D, based on the average line width with the follow equation.

$$\overline{\Gamma} = Dq^2 \tag{II.4}$$

$$q = 4\pi\lambda \sin\left(\frac{\theta}{2}\right) \tag{II.5}$$

where

q = Magnitude of the scattering vector

θ = Detection angle (90^o)

Using the Stokes-Einstein equation, we can then calculate the hydrodynamic radius, R_h, for particles in solution.

$$R_h = \frac{k_B T}{(6\pi\eta D)} \qquad \text{(II.6)}$$

where

k_B = Boltzmann constant

T = Temperature, absolute

η = Solution viscosity

2.13.2 Static Light Scattering

Static light scattering differs from dynamic light scattering based on two principles. One, the technique depends on the average position of the particles, not their motion. Secondly, the scattered light collected is measured over a wide range of angles, not at a set angle. This measurement relies on a completely different system property than that of DLS, but should yield a similar particle size for the same sample[63].

From Guinier, if we have particles of any shape in a random orientation, of a dilute solution, the observed intensity is

$$I(s) = n^2 \exp\left(-4\pi^2 s^2 \overline{R_D^2}\right) \tag{II.7}$$

where

$I(s) =$ Intensity

$s = \dfrac{q}{2\pi}$

$\overline{R_D^2} =$ Average of R_D^2, the radius of the shape in direction D

By taking the natural log of equation II.7, we end up with

$$\ln I(s) = \ln n^2 - \frac{1}{3} q^2 R_D^2 \tag{II.8}$$

$$R_g = \sqrt{3\overline{R_D}} \tag{II.9}$$

where

$R_g =$ Radius of gyration

We can plot ln I versus q^2 to obtain the slope. The slope of the graph is the radius of gyration. Figure II-1 shows the region of data that is considered for the Guinier analysis. The radius of a spherical particle (referred to by Guinier radius) is related to the radius of gyration by

$$R_g = R\sqrt{\frac{3}{5}} \tag{II.10}$$

where

$R =$ Guinier radius

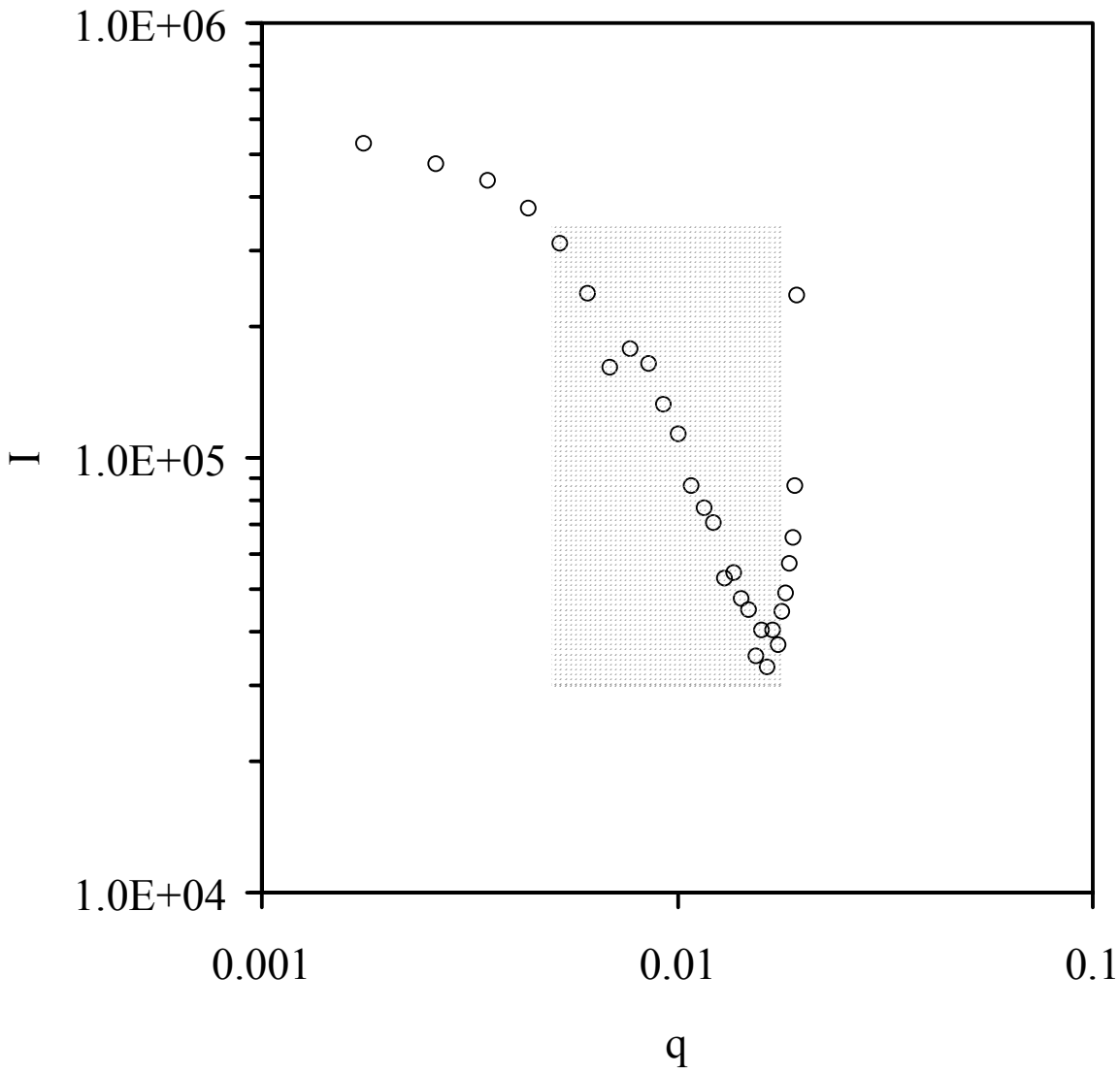

Figure II-1: Plot of I versus q for a given sample. This graph shows the intensity as a function of angle. By looking at the data as they approach low q, we can get the size of the particle. In the analysis of this sample, the first data points are excluded. The grey box indicates shows the region of the Guinier fit. The form factor equation is overlaid onto the data and the radius is adjusted until the points correspond accordingly.

Using the same collected data, another analysis technique that can be employed is fitting the entire scattering spectra to a geometric model; in our case, we fit the scattering data to a model for spherical particles. If the solution is monodisperse and dilute, the scattered intensity is given by

$$\Sigma(s) = \int_{V,\,particle} \exp(2\pi i s \cdot x) dv_x \tag{II.11}$$

$$\Sigma(s) = \frac{4}{3}\pi a^3 \Phi(2\pi s a) = \frac{4}{3}\pi a^3 \left[3\frac{\sin(qR) - (qR)\cos(qR)}{(qR)^3} \right] \tag{II.12}$$

$$I_F(s) = [\Delta\rho]^2 |\Sigma(s)|^2 \tag{II.13}$$

where

Δp = Scattering intensity

R = Radius, assumed

Equation II.11 is the Fourier transform of the form function, with the integral evaluated over the volume of the sphere. Once the integral is evaluated, we get the average value of the form factor over a given shape. Figure II-2 shows a general form factor graph. From this, we can get the form factor intensity for a particle of any given radius. The most distinctive attribute of the form factor are large minima in intensity that vary with particle radius. The radii from the Guinier analysis is input into the form factor equations to compare the location of the intensity minima with the collected data. The

utility in doing this is that for a given set of data, we can look at two distinct regions of collected intensities with different sets of assumptions to arrive at a consistent particles size.

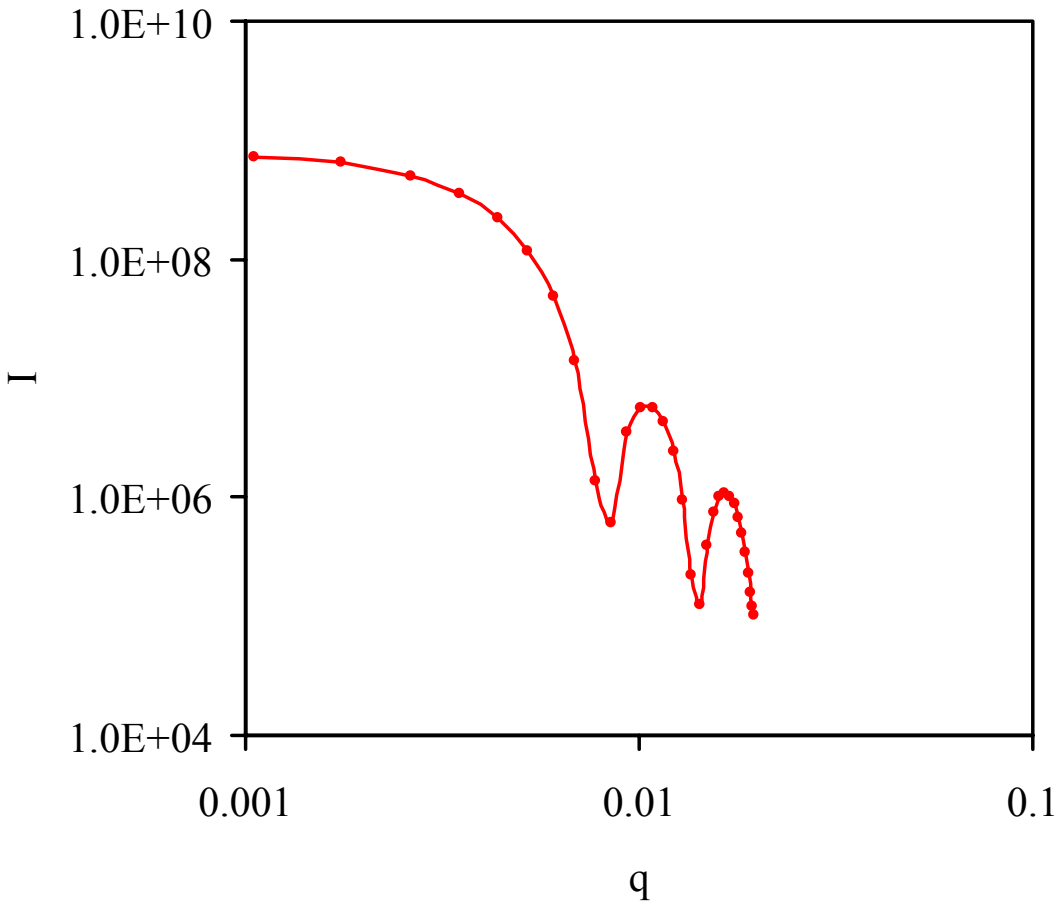

Figure II-2: Form factor graph for a particle of a given radius. This graph shows the form factor and the local minimums.

By looking at the small angle section, we can determine a particle size from the form factor equations. By looking at the middle range of angles, we can use the Guinier analysis to pick out the particle sizes. Hopefully, the two values should be close to each other, if not identical.

We can perform this analysis based on the fact that the vesicle interior has a different refractive index then that of the solution in which the particles are suspended. When present, an encapsulated polymer network offers a defined core in which the light can be scattered efficiently. For the polypeptide block copolymer vesicles, the solution on the inside of the vesicles has a different refractive index than that of the bulk exterior solution, but there is not set defined core, so the results tend to be less efficient at scattering light than those of the small synthetic vesicles.

2.14 pH Swings

For testing the polypeptide polymer vesicles response to pH changes, two solutions of acid and base were created. The acid and base were made with NaCl to keep the solutions iso-osmotic. The acidic or basic salt solution keeps the solution from changing osmotic pressure. The acid and base were added to the DLS and SLS samples to raise or lower the pH to either 7 or 11. The acid or base was added in, mixed in the same manner as the PBS was mixed with the original sample and placed back into their respective machines to be measured again. The acid for these experiments is HCl; the base NaOH.

2.15 Material Testing

Testing the tensile properties of the bulk polymer samples requires the follow equation[64]

$$E = \frac{Stress}{Strain} = \frac{FL_o}{A_o \Delta L} \tag{II.14}$$

where

$E =$ Young's modulus, Pascals

$F =$ Force applied to the sample

$L_o =$ Original length of the sample

$A_o =$ Original area of the sample

$\Delta L =$ Change in length of the sample

For the Young's modulus and compressive modulus tests, samples were prepared by making a large vial of polymer solution. Four vials were made, 5 and 10% solutions as well as 19:1 and 38:1 ratios. Photoinitiator and monomer was added to a custom made chamber consisting of a Teflon base with several holes of decreasing size drilled successively deeper. The smallest hole had a glass rod inserted and the largest hole had a plastic drinking straw inserted. This created an annulus for the polymer solution. Approximately 2-3 mL of polymer solution was added and placed under UV (250 nm) light for 2-3 minutes. The straw/glass group was removed from the Teflon based and placed in an iso-osmotic bath to help with the removal of the glass rod and the straw. The straw was removed first and fishing line was used to cut the polymer tube into

sections. Once the small polymer rings were cut, they were placed in another tray of iso-osmotic solution to wait for testing. Once all four polymer samples were created, the rings were tested on the Instron machine.

The Instron was setup for a tensile ring test configuration. The rate of pulling was held constant at 1 mm/min. Once the ring broke, another ring was placed on the arms, after the Instron returned to the starting position. During the test, the rings were assumed to be parallel rectangular samples, with the testing beginning with the sample in an unloaded state. When the strain gauge indicated a value of 0.1 N, the recorder started to record the values for the test.

For the compressive test, the same polymer solution was utilized, once again vortexed to ensure even distribution of the photo initiator. The same custom chamber was used, except this time no glass rod was inserted. This allowed for uniform cylinders to be created. The same steps were used in creating the cylinders as the rings, except a scalpel was used to cut the cylinders and trim off excess polymer gel.

The same Instron machine was used, except with a dynamic compressive test configuration. The rate of compression was the same as the extension, 1 mm/min. The machine started the recorder when the strain gauge indicated a value of 0.1 N. The gels were compressed to a strain of 10%, and then allowed to soak in iso-osmotic solution overnight. The gels were then tested to 20%, allowed to soak again overnight and finally test to failure at 40% strain.

For compression testing of the samples, equation II.14 is used, with the exception that E is now a compressive modulus, not a tensile modulus.

III. POLYMER ENCAPSULATION

3.1 DLS Test of Vesicles

Table III-1: DLS results from the extruded and freeze/thaw series.

Sample Name	Passes	Mean D	Relative Skew	Span of D
$E_{20}Bd_{33}$ Extruded a	5	200	0.048	198
$E_{20}Bd_{33}$ Extruded b	9	190	0.054	216
$E_{20}Bd_{33}$ Freeze/Thaw a	5	230	0.015	107
$E_{20}Bd_{33}$ Freeze/Thaw b	9	206	0.010	92
$E_{30}Bd_{46}$ Extruded a	5	278	0.875	624
$E_{30}Bd_{46}$ Extruded b	9	325	-0.067	110
$E_{30}Bd_{46}$ Freeze/Thaw a	5	332	0.287	375
$E_{30}Bd_{46}$ Freeze/Thaw b	9	308	0.487	83

The results in Table III-1 come from a set of experiments using both the polyethylene-b-polybutadiene ($E_{20}Bd_{33}$) polymer and the $E_{89}Bd_{120}$ polymer with a 10% AM-19 encapsulated inside. The recipe can be seen on Table II-2.

The experiment set out to determine what effect a set of freeze/thaw cycles would have on a sample before the sample was extruded. This experiment also sought to see how small of vesicles we could create. The number of passes through the extruder was also changed. From the table, we see that that freezing and thawing the samples before the extrusion makes the sample diameter variability smaller. This can be seen in the span of diameters and the mean diameters of the particles. With each sample, except for one, we see that extruded the samples for a few more passes, the average size of the particles decreases.

When comparing the $E_{20}Bd_{33}$ extruded vesicles versus the $E_{20}Bd_{33}$ freeze/thaw samples, we see the span of diameters is reduced from 200 to 100 nm. The diameters

seem about the same, 200 vs. 230. Comparing sizes with each subset of samples, we see the average size of the particles reduced.

For the $E_{30}Bd_{46}$ samples, using the same group as before, we see the span of diameters drop from 624 to 375 nm. The one outlier can be accounted for because of the large variance with the two samples. The $E_{30}Bd_{46}$ extruded sample has a large variance for the first sample, putting most of the data to the left of a normal distribution. The second sample has a negative skew, placing the bulk of the data on the right of a normal distribution. Both of these factors combine to make it seem that the particles average size increased with an increase of extruder passes. The $E_{30}Bd_{46}$ freeze/thaw sample shows a more normal distribution, as well as a smaller span.

3.2 Guinier Analysis of Vesicles

Table III-2: Guinier analysis and form factor results from the $E_{20}Bd_{33}$ and $E_{89}Bd_{120}$ series.

Sample Name	Guinier R	Form Factor R	Mean Diameter, Guinier
$E_{20}Bd_{33}$ Extruded N	136	140	273
$E_{20}Bd_{33}$ Extruded PH	129	129	257
$E_{89}Bd_{120}$ Extruded N	131	128	262
$E_{89}Bd_{120}$ Extruded PH	128	130	256
$E_{20}Bd_{33}$ Freeze/Thaw N	183	186	366
$E_{20}Bd_{33}$ Freeze/Thaw PH	138	138	276
$E_{89}Bd_{120}$ Freeze/Thaw N	99	99	198
$E_{89}Bd_{120}$ Freeze/Thaw PH	115	116	229

For the Guinier analysis, seen in Table III-2, all of the samples have been extruded 9 times, instead of varying the number of extrusion. The extruded has only been extruded, where the freeze/thaw samples went through a freeze/thaw cycle 5 times

before being extruded, just like the steps in the DLS test. The total concentration of polymer inside the vesicles was held at a constant 5%.

For this experiment, we altered the type of polymer encapsulated on the inside, switching between NIPAM and poly 1-hydroxy ethyl-methacrylate (PHEMA). We see that the different types of polymer encapsulated on the inside did not make a major difference in the mean diameter. This experiment was looking at determining if the type of polymer encapsulated in the interior of a vesicle would change the particle distribution or particle size. The difference with these monomer systems, compared with the acrylamide monomer (AM) is that they are not heavily crosslinked. Both monomer systems are still viscous. The AM system is heavily crosslinked, making a solid microgel in the interior of the vesicle, as compared to the NIPAM or PHEMA particles, which maintain a visco-elastic interior.

The sizes listed in Table II-2 are the result of doing a Guinier analysis, as outlined in the light scattering measurements section under the Methods section. The following graphs are the two graphs from the Guinier analysis as well as the form factor analysis. The first set of graphs are from a plain extruded sample; the second set is from a freeze/thaw sample.

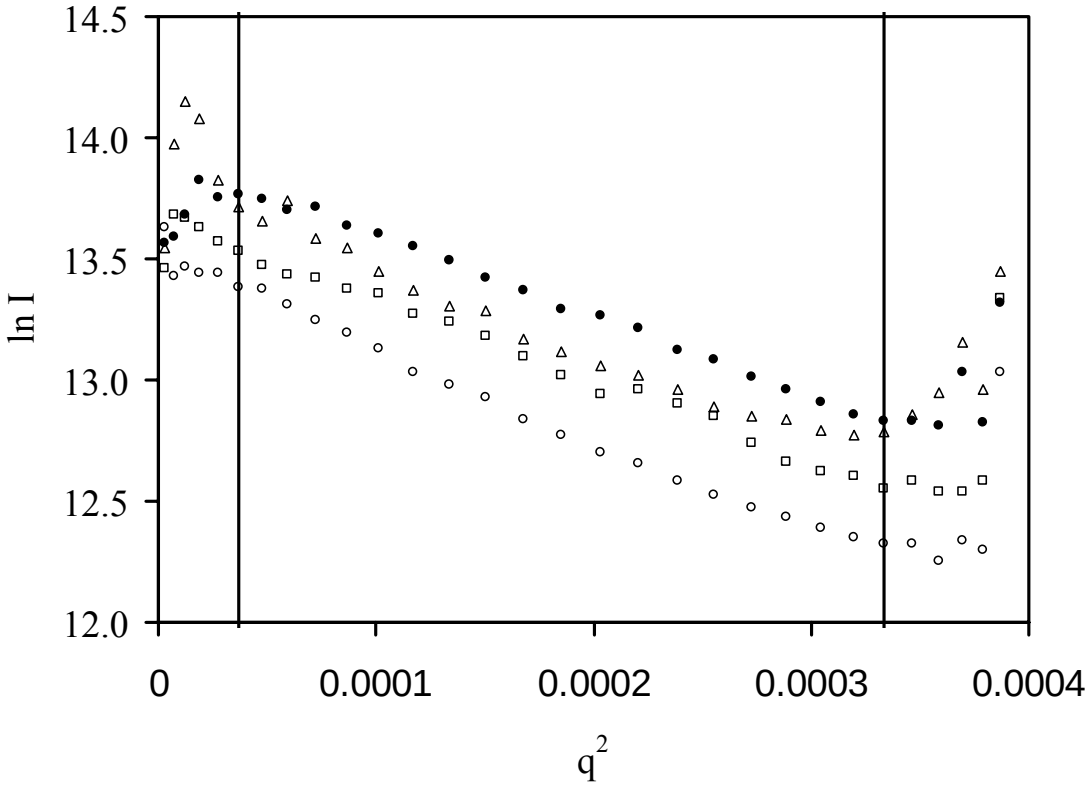

Figure III-1: The Guinier analysis of the extruded series. The data points for the four samples are as follows: open circles (○) are $E_{20}Bd_{33}$ Extruded N, the open squares (□) are E_{20}-Bd_{33} Extruded PH, the open triangles (Δ) are $E_{89}Bd_{120}$ Extruded N, and the filled circles (●) are $E_{89}Bd_{120}$ Extruded PH. The two black lines represent the area that was considered for the Guinier analysis.

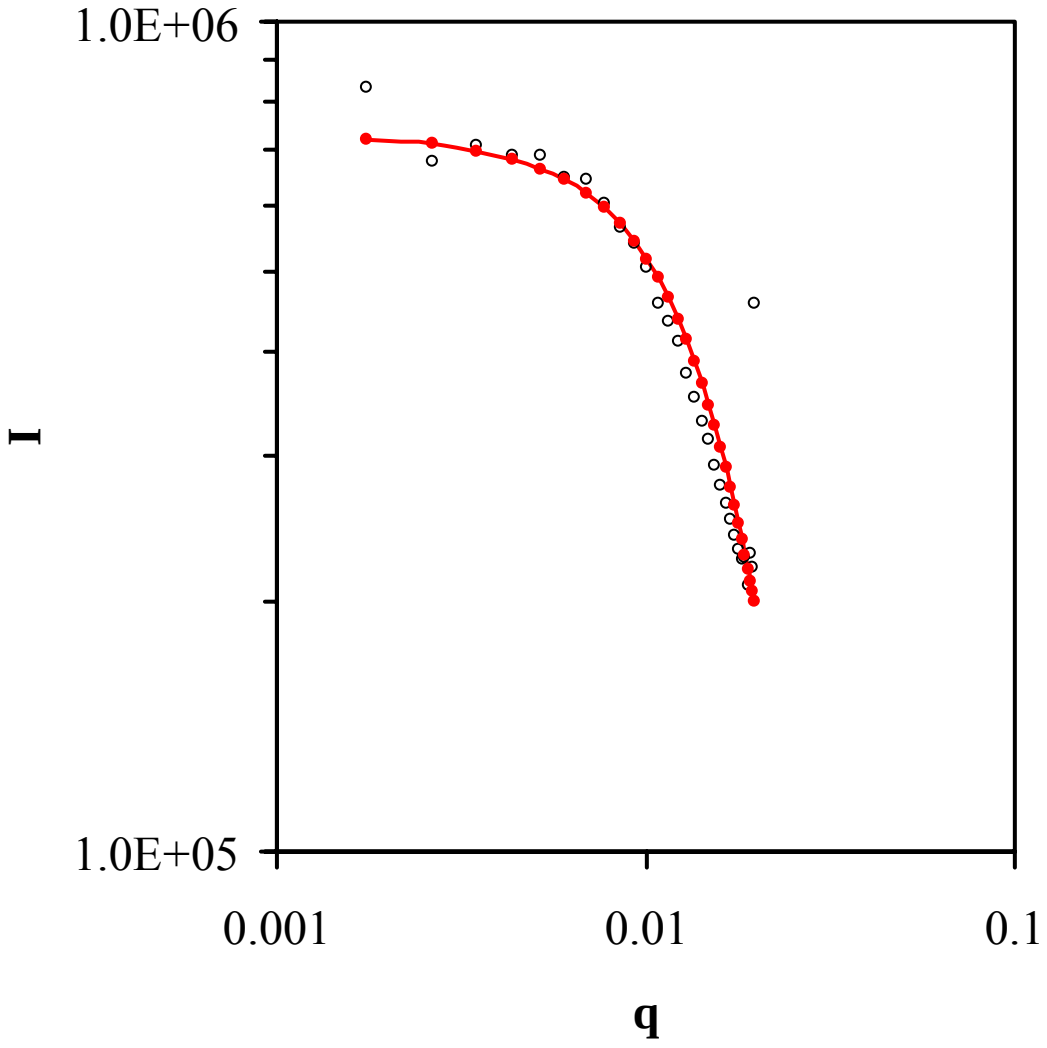

Figure III-2: Form factor graph. Here one of the samples is compared to a form factor equation. This is the $E_{20}Bd_{33}$ Extruded NIPAM sample. We see the form factor fitting the data almost completely. The minimum of the form factor here corresponds to a radius of 140 nm. The red line corresponds to the form factor equation.

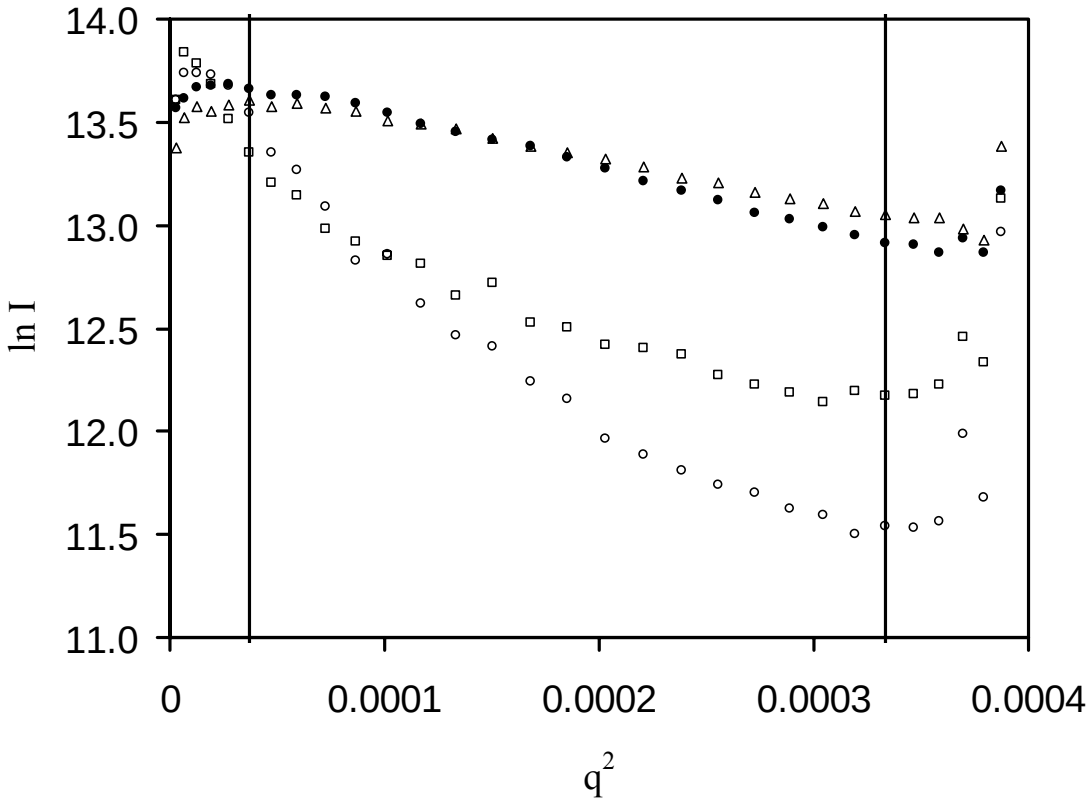

Figure III-3: The Guinier analysis of the freeze/thaw series. The data points for the four samples are as follows: open circles (○) are $E_{20}Bd_{33}$ freeze/thaw N, the open squares (□) are $E_{20}Bd_{33}$ freeze/thaw PH, the open triangles (Δ) are $E_{89}Bd_{120}$ freeze/thaw N, and the filled circles (●) are $E_{89}Bd_{120}$ freeze/thaw PH. The two black lines represent the area that was considered for the Guinier analysis, 55^{o} to 135^{o}.

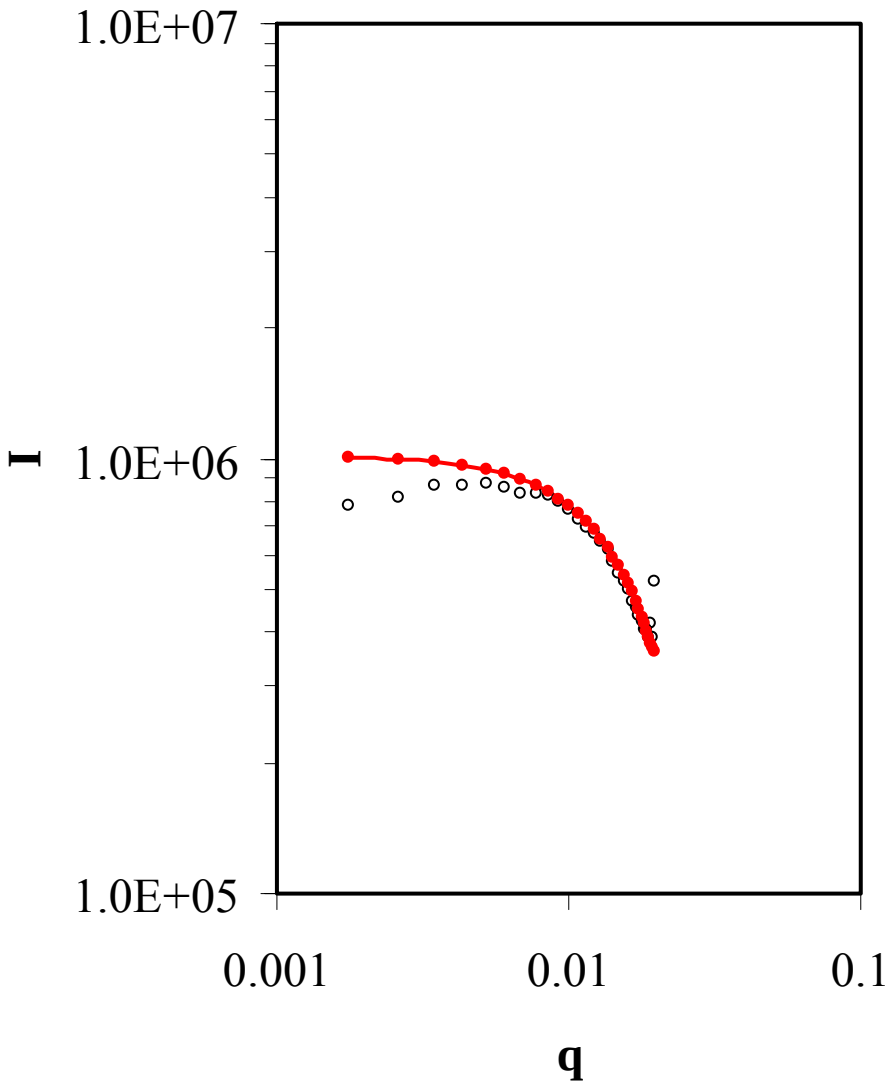

Figure III-4: Form factor graph. Here one of the samples is compared to a form factor equation. This is the $E_{30}Bd_{46}$ freeze/thaw PHEMA sample. We see the form factor fitting the data almost completely. The minimum of the form factor here corresponds to a radius of 116 nm. The red line corresponds to the form factor equation.

Figure III-1 and Figure III-3 shows the ln I versus q^2. From Figure III-1, we see that the extruded samples inside of the black lines are fairly linear. This gives us a good linear region in which the Guinier analysis will give reasonable values for the size of the particles in solution. For both the N and PH cases on the extruded series, the only

difference between the two systems is the bilayer polymer. All four radii are within limits of each other, indicating that an average size is achieved regardless of the polymer outside or the monomer inside of the vesicle. We see the form factor graph, Figure III-2, for the sample matches fairly well.

For Figure III-3, the freeze/thaw series was not as linear as the extruded series. As seen on Table III-2, the values are strikingly different from each other. The $E_{20}Bd_{33}$ freeze/thaw samples did not behave as the extruded series. It is unclear if the $E_{20}Bd_{33}$ samples were contaminated or if the vesicle structures failed before testing, giving scattered results. Since the $E_{30}Bd_{46}$ polymer was able to perform similar to the extruded trial, the $E_{20}Bd_{33}$ runs were probably contaminated. The $E_{30}Bd_{46}$ freeze/thaw samples performed almost identical, with the N sample having a smaller slope than the PH sample. The $E_{30}Bd_{46}$ solutions produced similar sizes in radii, with the freeze/thaw producing smaller average vesicles. Once again, we see the form factor graph, Figure III-4, showing good correlation.

For both experiments, the DLS and SLS report back values that are similar to each other indicating that we have the ability to control the size of particles as well as indicating that we might be partially successful with the encapsulation experiment. We can claim some success because of the fact that the particles scattered quite efficiently, as compared to the polypeptide block copolymer vesicles, explained in section 4. By looking at how the synthetic block copolymer vesicles scattered light and the intensity at which they did, we can be assured that the interior of the vesicle has a sequestered volume that has a vastly different refractive index than that of the bulk solution. When looking at the polypeptide block copolymers, the intensity of the scattered light is not

quite the same, giving rise to the idea that the refractive index is not as great as the synthetic vesicles. These results are indicative that the interior of the synthetic block copolymer vesicles have successfully contained and polymerized the encapsulated monomer in their interior.

3.3 SEM Photo of Freeze/Thaw Series

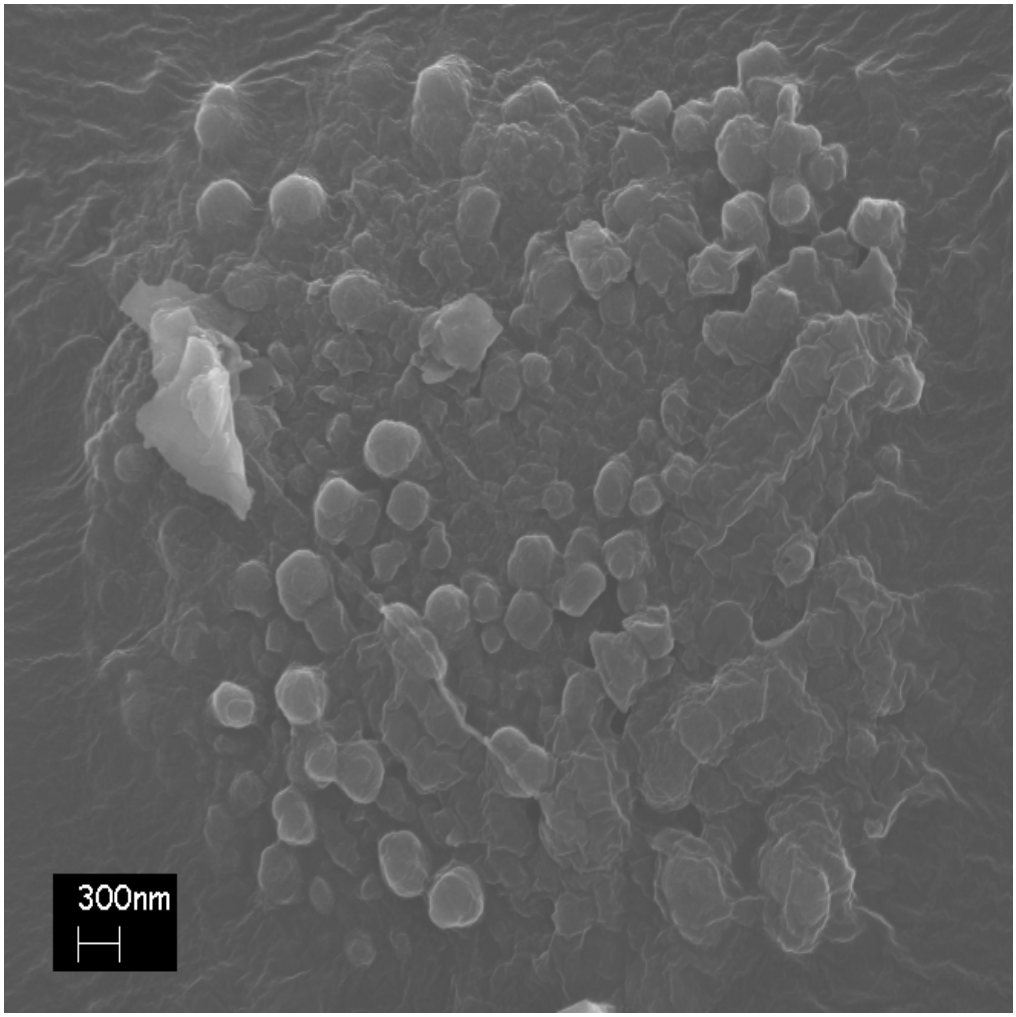

Figure III-5: A SEM photo of 200-400 nm particles. The small spheres are the remains of the acrylamide inside the vesicles.

A sample of the $E_{89}Bd_{120}$ freeze/thaw 10% AM particles were dialyzed against DI water for several days to remove as much of the sucrose and salt solutions present in the sample to be sent off for imaging. As stated before, SEM or TEM does not provide a good example of what structures are formed in solution, since the drying out process necessary for imaging destroys any self-assembly and the resulting image is that of aggregation of the polymer. In our case, we encapsulated in the interior of the vesicles acrylamide and then fully polymerized the vesicles to produce solid samples. The internal polymer network is not changed or destroyed due to those processing steps; the image from Figure III-5 is that of our final polymerized particles.

When the sample is dialyzed against DI and the sucrose or salt is removed from the sample, the vesicles will start to aggregate when the solution is dried. This is why the image has an island of polymer with the individual remains of a vesicle protruding from the surface. From the scale bar, we see that most of the acrylamide microgels are around 300 nm.

3.4 Dual Color Encapsulation

During this experiment, we were able to encapsulate acrylamide with a fluorescent marker inside an $E_{89}Bd_{120}$ vesicle. We have been successful in encapsulating fluorescent monomer into the interior of a vesicle as seen with the next section, interior polymer networks. From that success, we attempted to see if we could encapsulate the same monomer with the addition of a small amount of modified synthetic block copolymer that would be available to undergo chemical reaction to link a fluorophore to the copolymer. The interior network was a 10% AM-F network with 10% of the $E_{89}Bd_{120}$

polymer being acid polymer. Once the vesicles were created, dialyzed, and then polymerized, a coumarin-based dye was attached to the acid polymer. The resulting two-toned images, Figure III-6, are from the vesicle sample.

We can now make, with the synthetic block copolymer system, a vesicle with an adjustable surface chemistry, simply by changing the amount of acid polymer that is added to the normal synthetic block copolymer. We can now make a vesicle that possesses both a hollow membrane structure as well as a structure that possesses adjustable surface chemistry. The next section discusses the steps to create an internal polymer network that offers the ability to tailor a specific mechanical property. The only drawback to using the synthetic system is that in polymerizing the internal network, the fluid bilayer attribute is lost. The butadiene block in the copolymer polymerizes with itself and causes the hydrophobic region to become rigid. This is an advantage, as it makes the sample more robust so that it can undergo the linkage chemistry, but it sacrifices the fluid nature of the bilayer interface.

Upon doing a control experiment with identically created polymerized microgel vesicles, the coumarin dye was unable to offer the same results as the chemically linked vesicles. One explanation for this is that once the bilayer of a vesicle is polymerized, it is difficult to get hydrophobic dye to solubilize inside of the bilayer. Some residual coumarin was found in the bilayer, but not the same amount or intensity as the chemically linked vesicles.

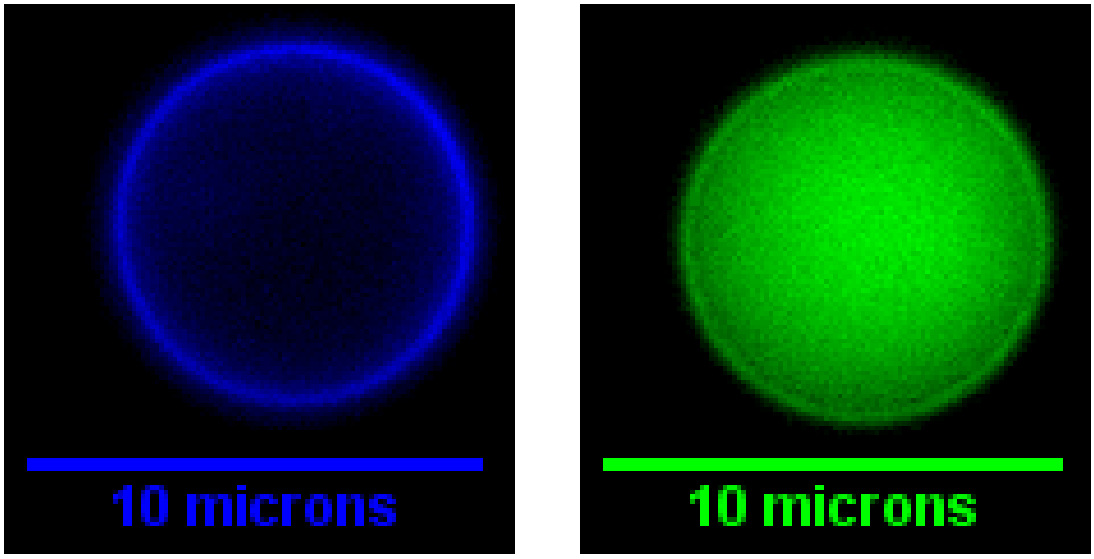

Figure III-6 : $E_{89}Bd_{120}$ with 10% $E_{89}Bd_{120}$-COO^- and 10% AM-19-F. Karym Kinnibrugh did the reaction to link a coumarin based dye with the acid polymer inside the vesicle bilayer. The reaction details are discussed in section 2.5. The coumarin dye, left, is linked to the acid polymer in the bilayer of the vesicle. The FITC, right, is integrated into an internal polymer network inside the vesicle. This is the same vesicle pictured for both images.

3.5 Interior Polymer Networks

One of the main goals of these experiments was to encapsulate monomer in the interior of a vesicle and polymerize it, giving the vesicle an interior polymer network. The internal polymer network will give us the capability to tailor specific mechanical properties desired for the biomimic. We can change these mechanical properties by changing the monomer encapsulated, the concentration of the monomer and the crosslink density of the monomer. With these widely adjustable parameters, we should be able to create a polymer network that can be either elastic or viscous, depending on the desired mechanical properties.

For this experiment, six sets of vesicles were created. All vesicles were created following the normal vesicle creation procedure, but four of the samples had acrylamide encapsulated into the interior of the vesicle. The acrylamide monomer concentration was changed, giving the vesicles both 5% and 10% in the interior. The crosslink density was also varied, both 19:1 and 38:1 ratio, monomer to crosslink. A fluorescent dye was incorporated into the internal polymer network to make imaging possible. The last two samples are controls with the fluorophore Nile Red incorporated into the bilayer. One of the last samples underwent polymerization of the bilayer, while the other remains fluid. All six samples were imaged and later, the values of each vesicle's height, width and contact length with a glass coverslip were measured. These data points are used for image analysis as well as mechanical analysis, as discussed in the next section.

For the various profiles of the vesicles in this experiment, we see an interesting trend. The amount that the vesicle lays down on the surface changes due to various levels of polymerization and encapsulation. In Figure III-7, we see this progression. The upper left picture is a vesicle without polymerization. The upper right picture is one that has only the butadiene in the block copolymer polymerized; in effect, polymerizing just the vesicle bilayer. The lower left picture is of an encapsulated vesicle, one with at 10% solution of AM-F at the 38:1 crosslink density. Finally the last picture, lower right, is of a 10% solution AM-F, but at the 19:1 crosslink density. We can see the vesicle sit less and less on the surface as the degree of polymerization and networking increases.

With the acrylamide encapsulated vesicles, we see that we have indeed encapsulated polymer on the interior of the vesicle. This proves we can indeed change the mechanical properties of the internal polymer network, since we can change the

concentration, crosslink density and the type of monomer we encapsulate. The next step is to determine the various moduli for the different monomer systems. The mechanical testing of the monomer systems is discussed in section 3.7.

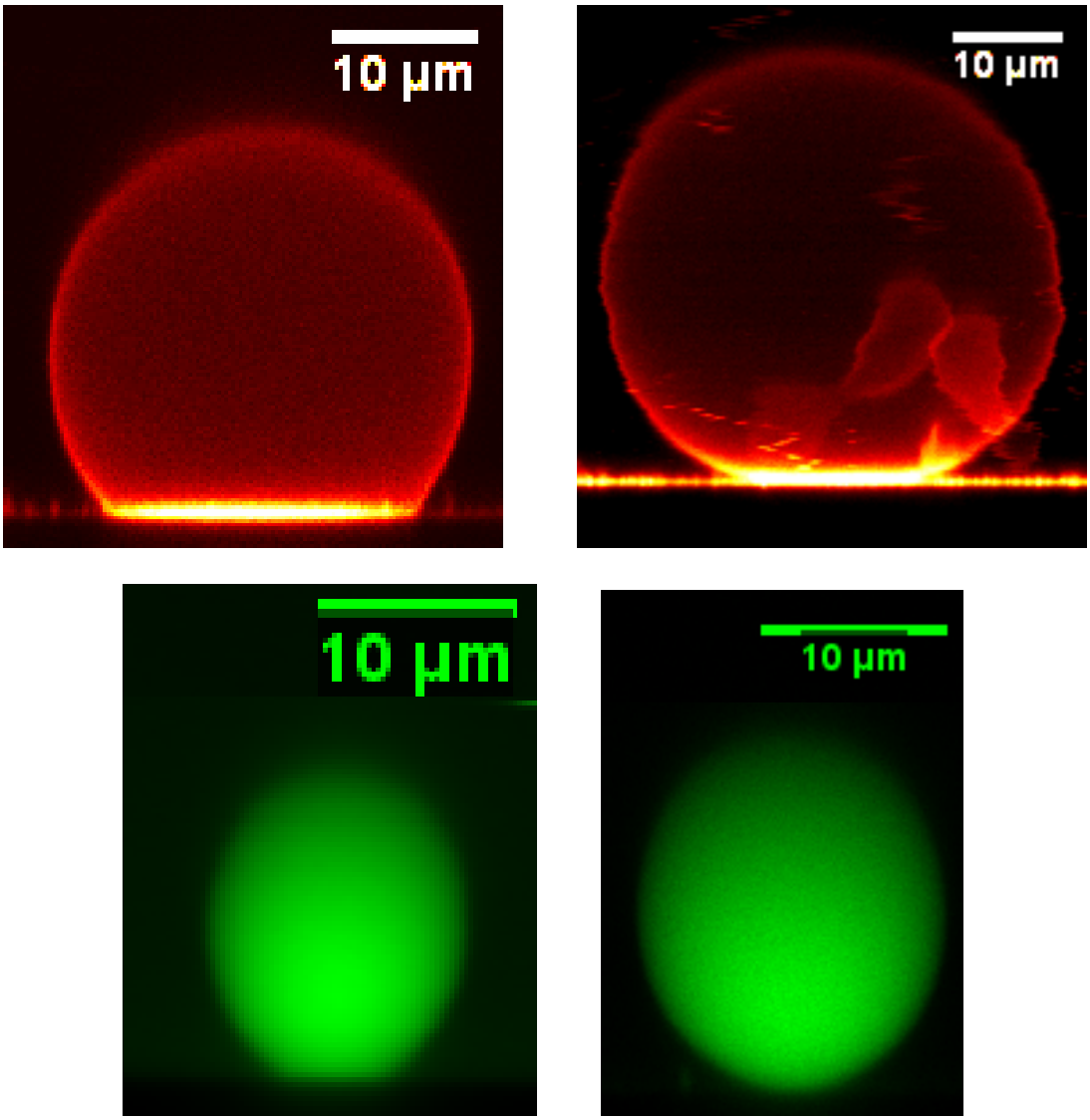

Figure III-7: The progression of polymerization on vesicles. The upper left picture is a vesicle with Nile Red embedded into the bilayer but unpolymerized. The upper right picture is a vesicle, made from the same technique as the previous picture, but has the bilayer polymerized. The lower left picture is a vesicle with 10% AM-F that has a 38:1 crosslink density. The lower right picture is of a 10% AM-F vesicle with a 19:1 crosslink density. Notice how the vesicle becomes more laid out on the surface as the amount of polymerization done to the vesicle decreases.

3.6 Image Analysis

Once the pictures were taken of the various polymer encapsulation tests, three variables were collected from the images: the height of the particle, the width of the particle and the length of contact to the surface of the particle. Using geometric equations, we can calculate the volume of the particle, as well as the depressed volume. The follow equations were used in order to calculate the various parameters.

$$d = a\left(1 - \left(1 - \frac{y^2}{b^2}\right)^{0.5}\right) \tag{III.1}$$

where

d = Depression depth of particle

y = Contact length, divided by two

a = Radius of major axis

b = Radius of minor axis

$$V = \frac{4}{3}\pi b^2 a \tag{III.2}$$

where

V = Total volume of particle

$$V_d = \pi b^2 d - \frac{\pi}{3}\left(\frac{b^2}{a^2}\right)d^3 \qquad \text{(III.3)}$$

where

V_d = Depressed volume

$$y_{Normalized} = (a-d) + a\sqrt{\left(1-\frac{x}{b^2}\right)} \qquad \text{(III.4)}$$

where

$y_{Normalized}$ = Normalized contact length, divided by two

The pictures are categorized into two categories. The first is fully polymerized particles and the second is partially polymerized or shell polymerized particles. This is apparent by looking at the various profile pictures of the particles. Figure III-8 shows what a particle that is not completely polymerized.

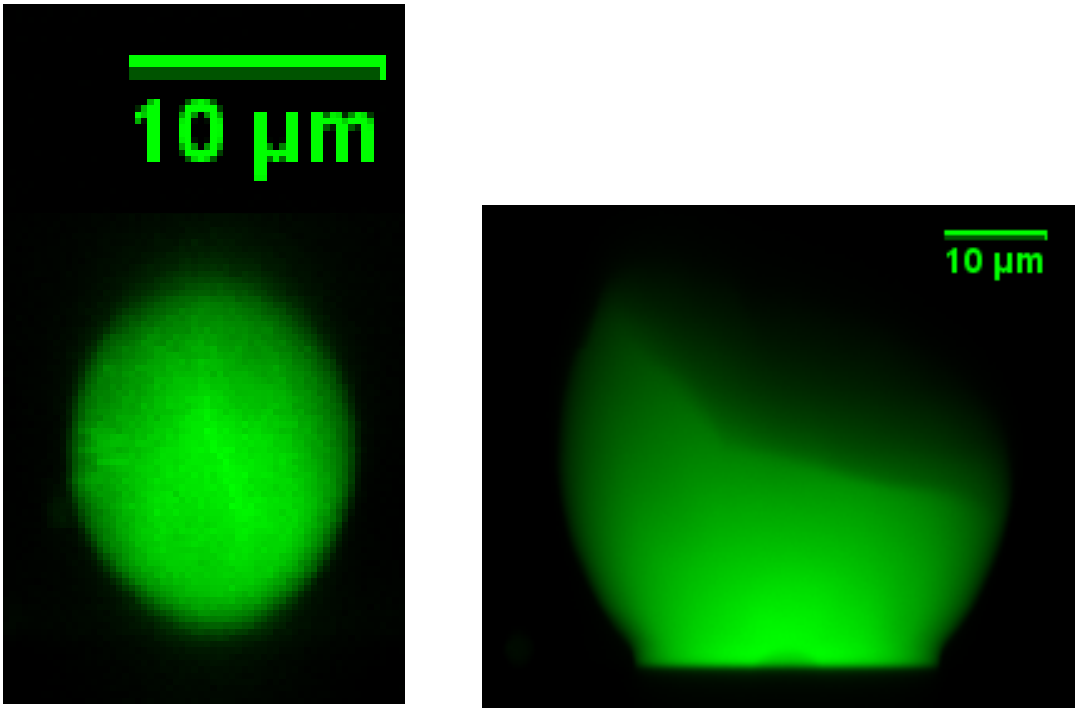

Figure III-8: Unpolymerized vesicles. The vesicle on the left hand side is a 19:1 ratio vesicle that is not fully polymerized. Notice the dark spots on the interior of the vesicle. The right hand picture is a 38:1 ratio vesicle that is unpolymerized as well. The large, dark region at the top indicts no fluorescence is present.

Following the Hertz's analysis outlined by Liu[(65)], we see the fully polymerized particles follow the Hertz theory fairly well. Hertz theory makes the assumptions that the sphere is perfectly elastic and there are no interactions, either adhesion or friction, between the sphere and a contacting plate or two spheres in contact. Hertz theory has been proven valid for small deformations of solid spheres, since in the small deformation limit, most solids are perfectly elastic. Using equation (1) from Liu's paper, we can plot contact area versus volume for the various particles. We should see a cubic relation between the volume, which can be converted into weight, and the contact length of the particle on glass. Some of the particles, when plotted, did not follow the cubic function.

In order to explain what was happening with those particles, another theory was explored – JKR theory.

JKR theory is a similar theory to Hertz, but includes a surface energy based interaction between the sphere and flat surface. Here adhesion between the sphere and contact surface accounts for the deformation of the particle, instead of the weight of the particle. Following the same analysis for Hertz theory, the particles should still scale with $W \sim a^3$. This indicates the scaling has more to do with the structure of the particles rather than the origin of the deforming force. To investigate how JKR theory was affected by changes in the particle structure, the theory was further modified by Shanahan[66].

Shanahan switched the particles from JKR theory from solid spheres with adhesion to hollow "balloons" with a deformations and small internal pressures. Shanahan outlines a model case of a large elastic balloon with an internal pressure and deformed slightly on a surface. This best describes the situation of our particles when they are not polymerized. The vesicle bilayer can deform extensively, but the surface tension exerted by the interaction of the polymer within the bilayer yields a large, thin walled elastic "balloon". If the shell is fully polymerized, the shell forms a rigid membrane; no longer possessing a fluid hydrophobic region. The resulting mechanical properties resemble that of a solid particle (under small deformations). It is expected the shell nature of the particle would be evident under larger deformations. Making these assumptions from Shanahan, the scaling law changes from $W \sim a^3$ to $W \sim a^2$.

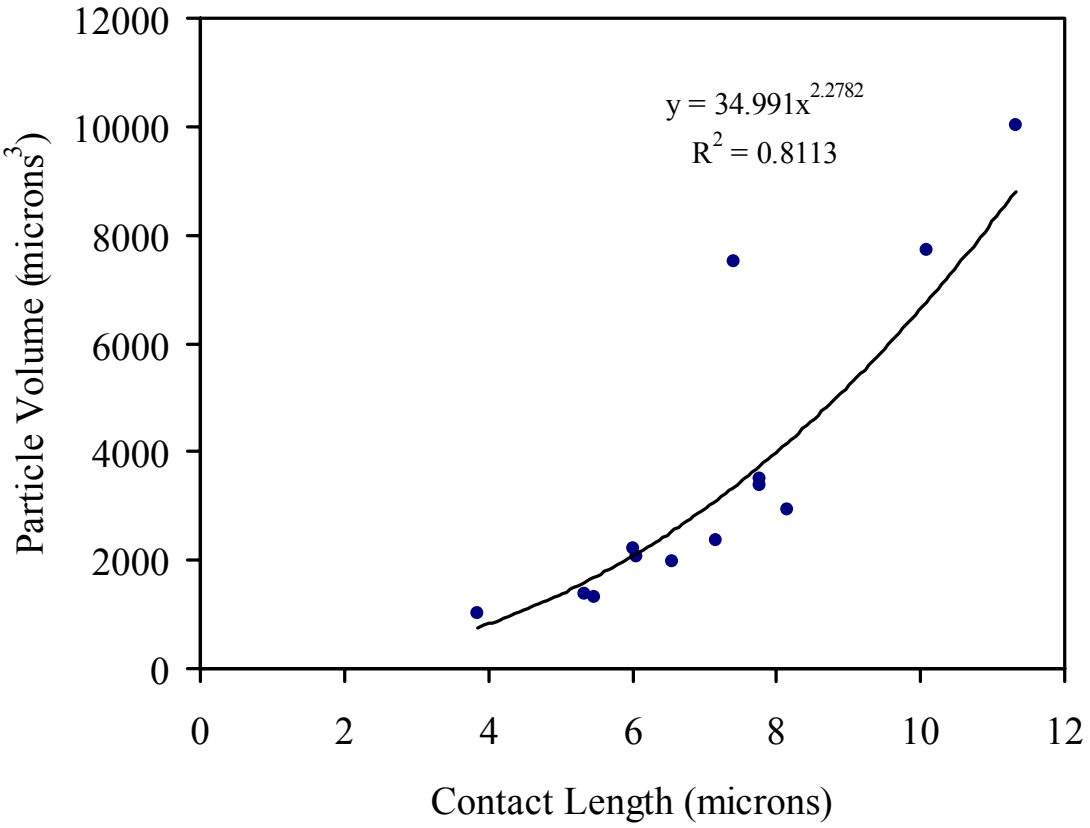

Figure III-9: JKR analysis on the unpolymerized particles. We see the particles correspond to a quadratic, which corresponds to the "balloon" theory.

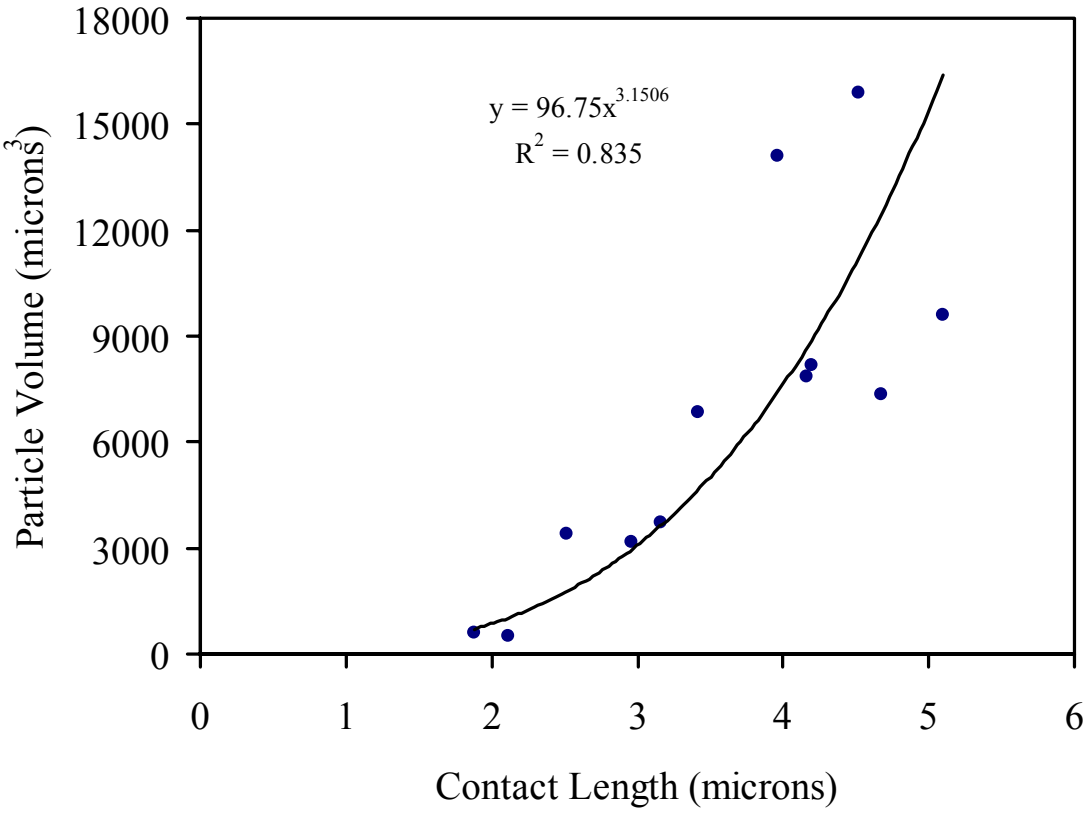

Figure III-10: Hertz analysis on the shell polymerized particles. These shell polymerized particles act in a manner similar to fully polymerized particles at these deformations.

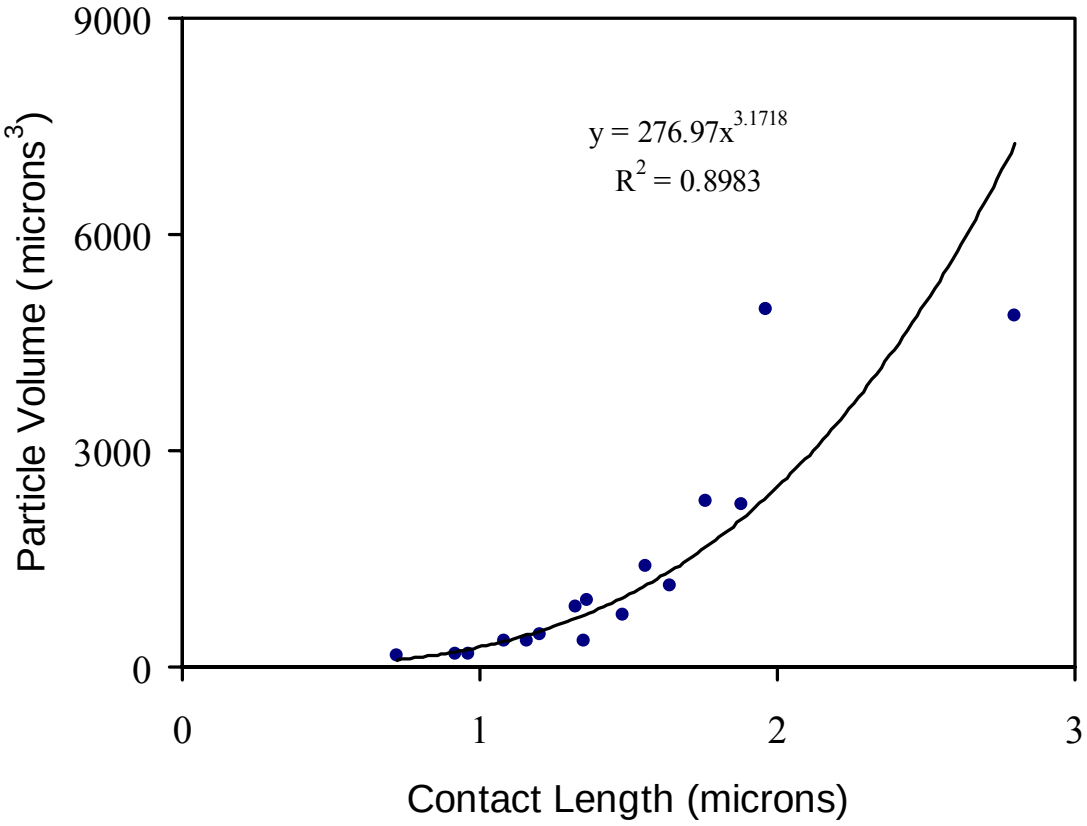

Figure III-11: Hertz analysis on the 38:1 particles. We see the particles correspond to a cubic, which corresponds to the Hertz theory.

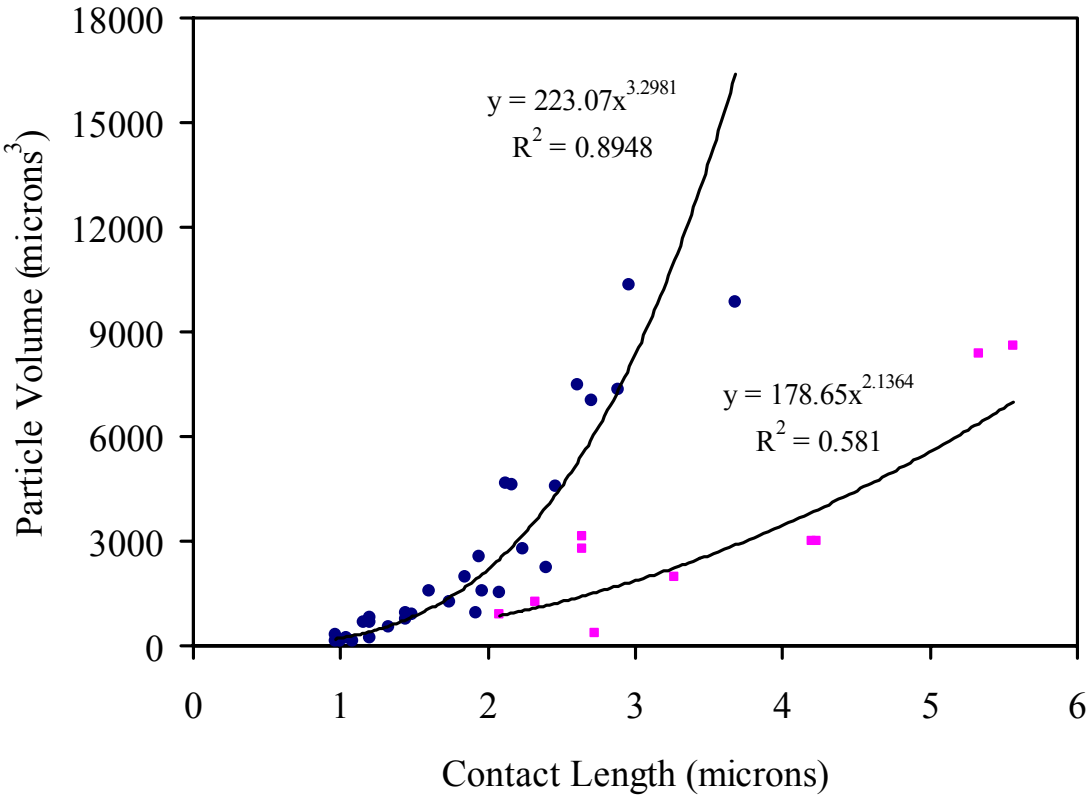

Figure III-12: Mechanical analysis on the 19:1 particles. The blue circles are the solid particles, following Hertz theory. The pink squares correspond to partially polymerized vesicles.

Figure III-9 shows the response of unpolymerized, normal vesicles. Looking at the plot of the volume to contact length, we see they follow a quadratic function. This mirrors the theory set forth by Shanahan for the "balloon" particles. Since the particles have no polymerization or crosslinking of the membrane, we have a fluid vesicle, easily deformable and soft.

In Figure III-10, the particles are the shell polymerized vesicles. These particles have had the double bonds in the polybutadiene crosslinked to each other. The resulting particle can be thought of as being similar to a ping pong ball – a solid shell enclosing a

fluid. Thinking of the example, one might think that the particles response would be similar to the "balloon" theory, an elastic membrane that responds according to a^2. However, the observed response is that of a solid Hertz response, a^3. Under the deformations observed, we see no qualitative difference between a solid shell and a solid particle.

If the solution had an osmotic pressure difference, that could affect the particle slightly. Polymerized shell vesicles are still somewhat deformable, shown by Discher[16], and if the osmotic pressure was lower on the exterior of the vesicle, we would expect to see the vesicle laying down more on the glass than if the osmotic pressure was equalized. If the osmotic pressure was higher on the outside, we would expect to see the particle sitting less on the glass, to accommodate the extra volume by trying to stretch the membrane. Since the osmotic pressure of the exterior bulk solution is always lower than that of the internal solution, we should have a particle lying down on the glass more. The difference in osmotic pressure should change the overall internal pressure of the particles.

For Figure III-11, we see that the particles response as a solid, elastic sphere. The response is not as great as the 19:1 sample, Figure III-12, but the crosslink density is only half the 19:1 sample. These particles responded as expected, similarly as the unpolymerized vesicles.

For Figure III-12, we see two distinct sets of data points. The blue data points correspond to particles that are completely polymerized. This is seen both in the profiles, sitting high on the surface of the glass with very little deformation of the contact area. The second set of data points correspond to vesicles that are unpolymerized. It is not

clear why some vesicles remain unpolymerized within this sample to yield two sets of data with a single sample.

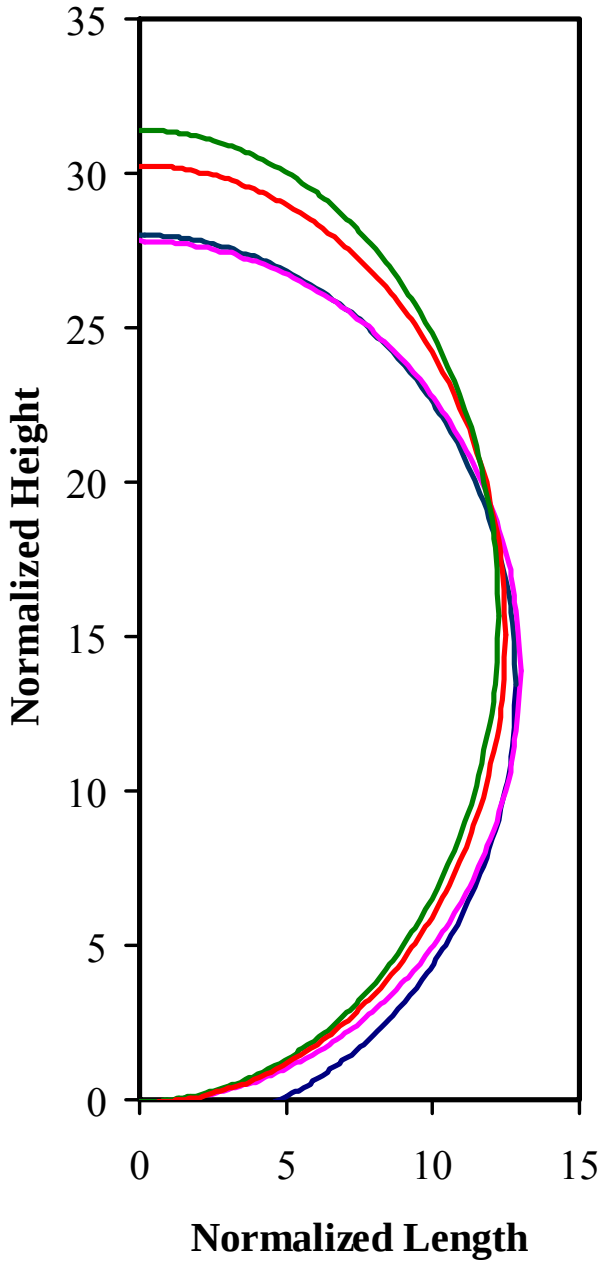

Figure III-13: Normalized profiles of particles. Here we have the normalized profiles of the four cases of polymerization: the blue line (●) is the unpolymerized particles, the pink line (●) is the polymerized shell particles, the green line (●) is the 38:1 acrylamide particles and the red line (●) is the 19:1 acrylamide particles.

Looking at Figure III-13, we see the profiles of the four cases of polymerized particles. The plots have been normalized so that each half profile encloses the same volume particle. This plot confirms that as the material on the interior of the vesicle is increased in rigidity; the particle stands taller on the glass, rather than laying flat. The polymerized shell has much less surface contact area than the unpolymerized shell, most likely because the stress of the sharp local curvature at the contact line between the particle and glass is distributed across the solid shell network. When an internal polymer network is encapsulated inside the vesicle, the profile changes dramatically. The contact area is still smaller than the unpolymerized particle, but the normalized height of the particle is taller than the polymerized shell. This indicates that the properties of the interior network will affect the overall shape of the particle when it is in contact with a surface. Under the conditions tested here (small forces and deformations) we cannot discern a difference in between the two crosslink densities. However, it is expected that there would be different resistances to deformation at higher forces between the different crosslink densities, as there is a difference in between the polymerized shell and solid particles at these forces. This proves to be promising because of the properties desired to be built into the particle. Having a particle that is deformable to a degree, and then resists any additional deformation is trait representative of a cell. This allows the particle to have some contact area, but still can hold up to the forces that could be applied to the vesicle in solution.

The profile plot gives us some indication of what to expect when the internal polymer network undergoes material testing. This analysis is useful to see the varying

degrees of contact area with varying internal components, but it does not give us any values that we can compare. For this, the internal polymer network was tested in both compression and extension.

3.7 Material Tests

Table III-3: Material moduli for 5% AM. All values are in units of pascals.

Crosslink Density	Young's Modulus	Compressive Modulus
19:1	3080 ± 1080	8400 ± 1350
38:1	2600 ± 660	4880 ± 1080

Table III-4: Material moduli for 10% AM. All values are in units of pascals.

Crosslink Density	Young's Modulus	Compressive Modulus
19:1	22000 ± 1820	38620 ± 9400
38:1	14970 ± 3800	15780 ± 5250

Looking at the bulk Young's moduli for the two cases in Table III-3 and Table III-4, we see that the moduli do not scale by a simple factor. In the Young's moduli for the 5% concentration samples, the two values are nearly identical. This can be explained by the low concentration of polymer and the large concentration of water. Under extension, the polymer chains are less likely to encounter other polymer chains, making it hard to build up a completely continuous polymer network. The minimum gelling concentration for acrylamide has been experimentally determined to be between 1 and 4%.

For the 5% concentration, the compressive modulus is about twice as much for the 19:1 compared to the 38:1. This sample shows that as we double the crosslink density, the compressive modulus follows a similar trend.

In the 10% concentration case, the values are quite different from each other. For the compressive modulus, the 19:1 is about two and a half times the modulus for the 38:1. We see that doubling the crosslink density once again gives us almost a similar doubling in the compressive modulus. Since the standard deviation of the 19:1 sample is quite large, the effect of doubling the crosslink density may be close to just two times the compressive modulus, and not two and half times.

For the Young's modulus, the value for 19:1 differs by only 66%. The difference in the two sets of numbers and how they are not linearly related can be explained by the large amount of water in each sample. These samples still have large percentage of water making up the sample volume. For the 10% polymer concentration case, the polymer should be able to make a single, continuous polymer network. Having the continuous network will allow the sample to undergo larger strains.

Looking at the same crosslink density samples, but changing the polymer concentration, we see an interesting trend. For the 19:1 ratio, as we increased the polymer concentration for 5% to 10%, we see the values for the Young's modulus increase seven-fold. The values for the compressive modulus increase almost three-fold. What is interesting is that the same increases in values are seen with the 38:1 ratio. Both sets of values increase at the same rate as the 19:1. The end values are smaller than that of the 19:1, but the lower concentration values were lower to begin.

At the small strains that were investigated, the polymer network was not strained past the reversible, elastic point. As the strains were increased, the polymer network was stressed, as well as the gel expunging the water from the network. Because the crosslink

density can affect the way the polymer network retains water, when the strain is applied, the water can leave the sample at a varying rate.

The reported values are of all the tests conducted on the cylinders. Three overall tests were performed: a 10% compression, a 20% compression, and a 40% failure test. Figures A-1 thru Figure A-4 in Appendix A show the results from each of the individual tests.

IV. POLYPEPTIDE BLOCK COPOLYMERS

4.1 Circular Dichroism

Circular Dichroism (CD) was performed by Dr. Jeng Shiung of Dr. Shantz's group. The results are graphed in Figure IV-1 and Figure IV-2. We can see from the first graph, a polymer concentration below the critical micelle concentration (CMC), that as the pH is increases, we start seeing two distinct peaks, one around 208 nm and the other around 222 nm. These two peaks correspond to an alpha helix being formed. Since the solution contains just free polymer chains, we know that the polylysine block is collapsing from a random coil into an alpha helix. While we cannot determine how much of the structure is converting into an alpha helix, or how fast it is converting, the main point is that the block polypeptide polymer is converting from a random coil into a structured material due to an increasing pH.

For Figure IV-2, the polymer chains are ordered into a structure, since we are now above the CMC. This causes the light from 190 nm to 208-209 nm to be scattered. This makes it difficult to see the 208 nm peak, but we can still see the 222 nm peak. Once again, as the pH is increased, the definition of the peak is increased.

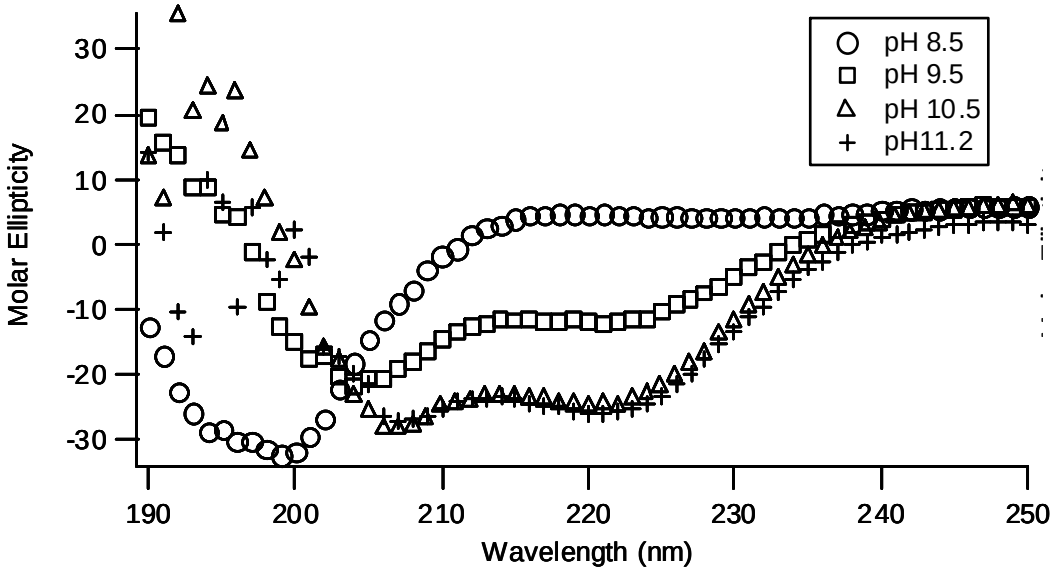

Figure IV-1: Circular dichrosim for K110-b-G55 as a function of pH at 1.16 μM. This concentration is below the CMC. We have the dual peaks at both 208 and 222 nm, indicating that the block copolymer is forming an alpha helix at higher pHs.

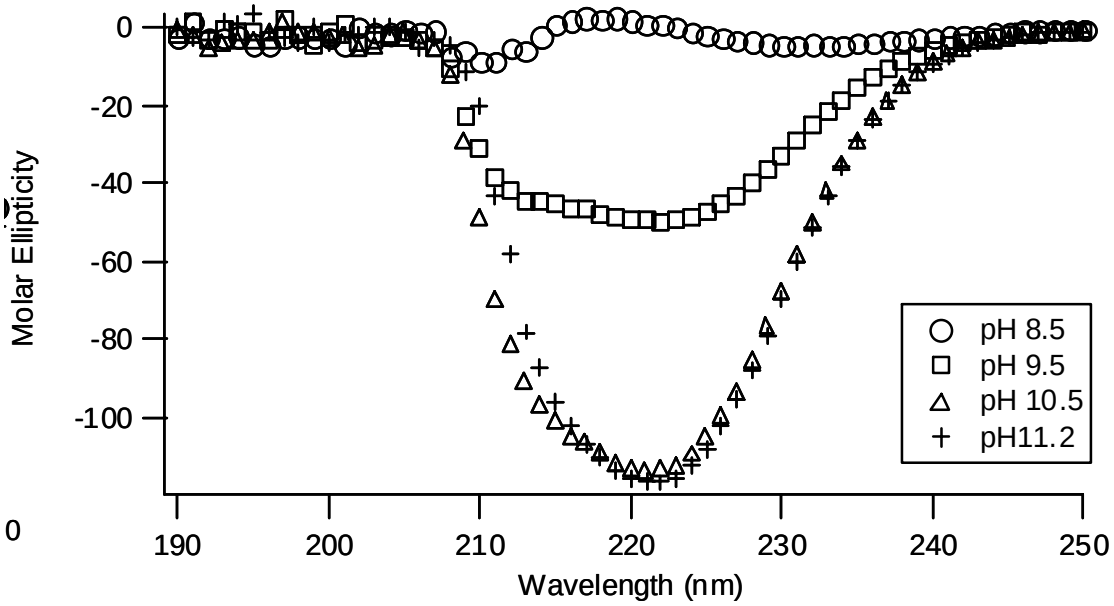

Figure IV-2: Circular dichrosim for K110-b-G55 as a function of pH at 4.05 μM. This concentration is above the CMC. The peaks indicating an alpha sheet are harder to see, but the figure shows a small peak around 222 nm, with the solution scattering the 208 nm peak.

4.2 Particle Sizes in Solution

After the CD experiment was completed, we needed to see if large of particles could be created in solution to enable imaging of the aggregates. Several methods of vesicle formation were employed, notably the standard vesicle creation technique and the alternative vesicle creation technique. Part of the drive for the various techniques was to determine and show that the vesicles being created were thermodynamically stable in solution, not a product of being kinetically trapped structures due to salt concentration or other factors. In Table IV-1, we see the hydrodynamic radius, R_h, and the Guinier radius, R. Rh is calculated from the dynamic light scattering experiment (DLS), and R is calculated from doing a Guinier analysis on results from a static light scattering experiment (SLS). $1/\kappa$, the Debye length, is also calculated to show the effect of increasing the salt concentration[67].

Table IV-1: Radii as a function of salt concentration. This is the values used for Figure IV-3, including the Debye length for the various samples. As the salt concentration increases, the Debye length decreases, as does the difference between the hydrodynamic radius and the Guinier radius.

[NaCl], M	$1/\kappa$, nm	R_h	R	ΔR
$1x10^{-5}$	96.1	302	149	153
$1x10^{-3}$	4.3	239	138	101
0.1	0.96	179	133	46
1.0	0.3	165	146	19

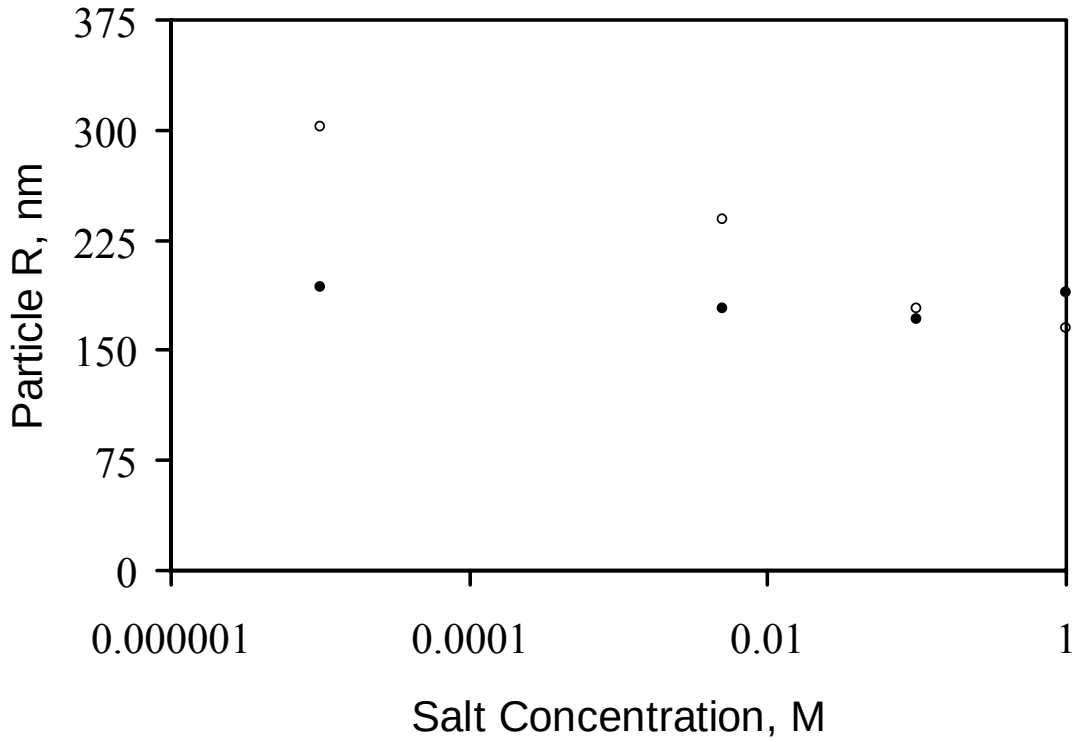

Figure IV-3: Hydrodynamic radius and Guinier radius as a function of salt concentration. The open circles (○) are the hydrodynamic radius, as measured by Jeng Shiung, in changing concentrations of NaCl. The solid circles (●) are the Guinier radius, as measured by the author, with the same varying concentrations of NaCl.

As the salt concentration increases, we see R_h approach the size of R. This is attributed to the amount of screening charges available to the Lysine block. As the concentration of salt decreases, the Lysine chains have to elongate in order to counteract the charges from the neighboring polymer chains. As explained by others[68-72], the effect of salt can change the way the polymer chains interact with each other in solution. The one basic assumption is that of the Donnan limit; the salt added to the solution screens any long range electrostatic charges the polymer may have with neighboring chains.

For vesicles, we assume that the polymer is an absorbed layer with the polyelectrolyte chains acting as the polymer brush. The hydrophobic core, in this case

the Glysine block, acts as a "molten film", an unresponsive block to changes in salt or pH. The Lysine brush will expand or collapse due to the decrease or increase in screening charges, in this case salt concentration.

When the salt concentration is low, the brush becomes an osmotic brush; the chains extend due the counterion pressure being exerted on the polymer chains. During the region of osmotic brushes, any slight variation in the salt concentration will not show any reduction in the length of the brushes.

As the salt concentration increases, the brushes cease being an osmotic brush and become a salted brush. Once in the salted brush region, the length of the brushes should scale as $L \sim c_S^{-1/3}$[72]. Looking at Figure IV-4, we see the difference in radius, the hydrodynamic radius minus the Guinier radius, decrease at the power of 0.38. Due to relatively few data points, this is considered a close correlation. The difference in the two radii should give us the characteristic length of the Lysine block in solution. As the Lysine block collapses due to an increase in salt, the hydrodynamic radius should, and does, decrease, giving a smaller blob sphere for the Lysine chains.

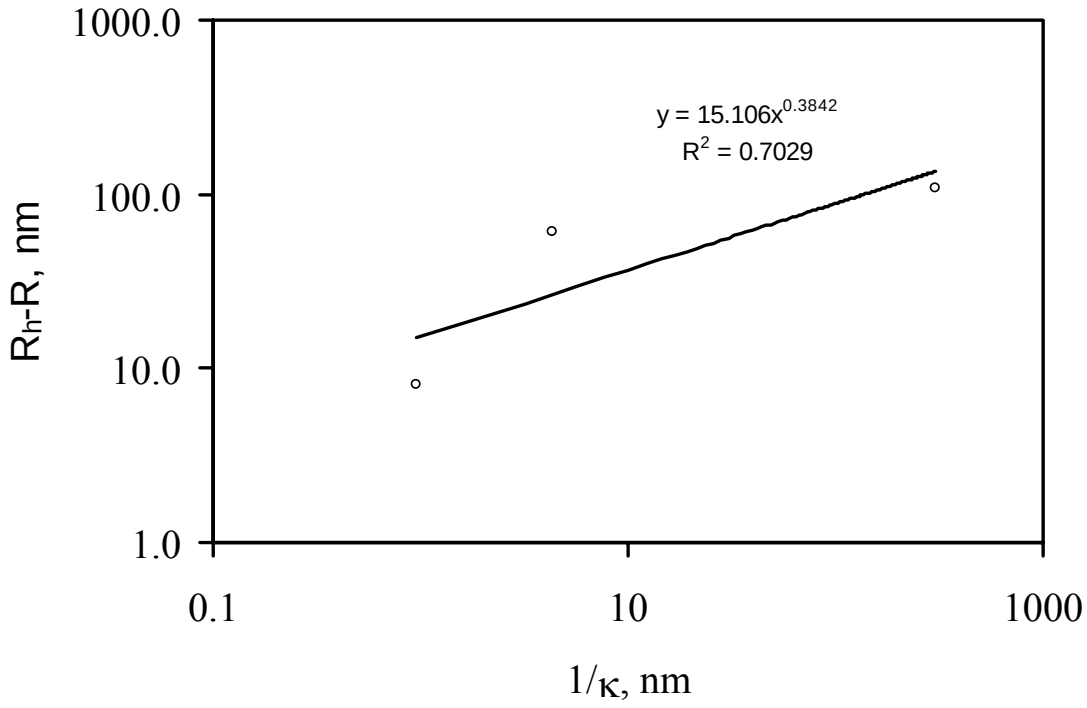

Figure IV-4: The difference between radii as a function of Debye length. Plotting the difference in hydrodynamic radius from Guinier radius as a function of the Debye length gives us a chain length reduction on the order of 1/3, which corresponds to Tirrell.

4.3 pH Swing

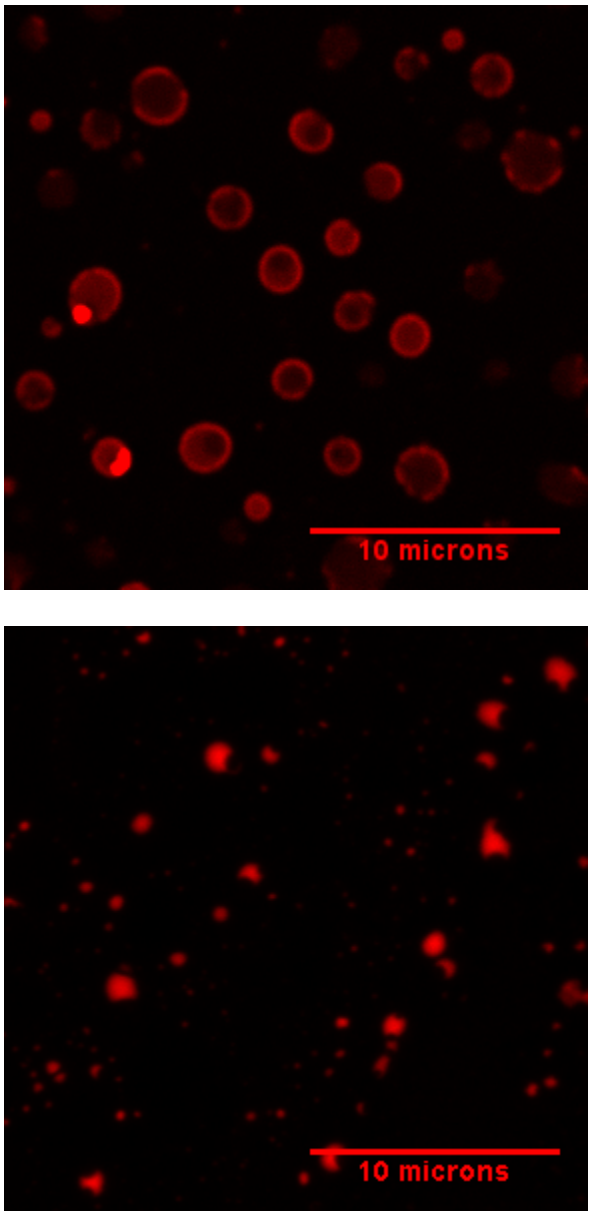

Figure IV-5: Confocal images of Lys_{200}-b-Gly_{50} at pH 7 and 11. The top figure is the solution at pH 7; the bottom image is the same solution, not the same view, at pH 11. The change in pH has caused a structural rearrangement that yields no vesicles on these size scales at pH 11.

For Figure IV-5, we see the affect of increasing the pH of a sample. The vesicles in the top picture are at pH 7. They form vesicles with a clear bilayer. The bottom picture is a picture of the sample after the pH has been raise up to 11. Here we see the polymer aggregating out of solution and forming large masses of polymer. The Nile Red is still incorporated into the polymer, but no longer do we see self-assembled bilayers.

To test the pH responsiveness of the polypeptide block copolymers, samples were made for both DLS and SLS. For DLS, the samples were made by the alternate vesicle formation method. For SLS, the samples were made with the standard vesicle formation technique.

The general trend for both samples is that the first cycle is higher than the other values of pH 7, and then hovers around an average value for the rest of the cycles. This can be seen on both Figure IV-6 and Figure IV-7. This can be explained as the vesicles, when first created, are of a large distribution. When the sample is first tested, the distribution of vesicle sizes is quite extensive. Once the pH has been raised to 11, the polymer starts becoming insoluble, forcing the vesicles to collapse. Once the pH has been returned to 7, the polymer becomes soluble again, but the vesicles cannot return to their original size. An average size of vesicles is eventually reached, after several pH swings. The resulting solution is more monodispersed than the original sample, unless the original sample has had additional processing steps performed. After raising and lowering the pH several times, the vesicles approach a size of 145 nm.

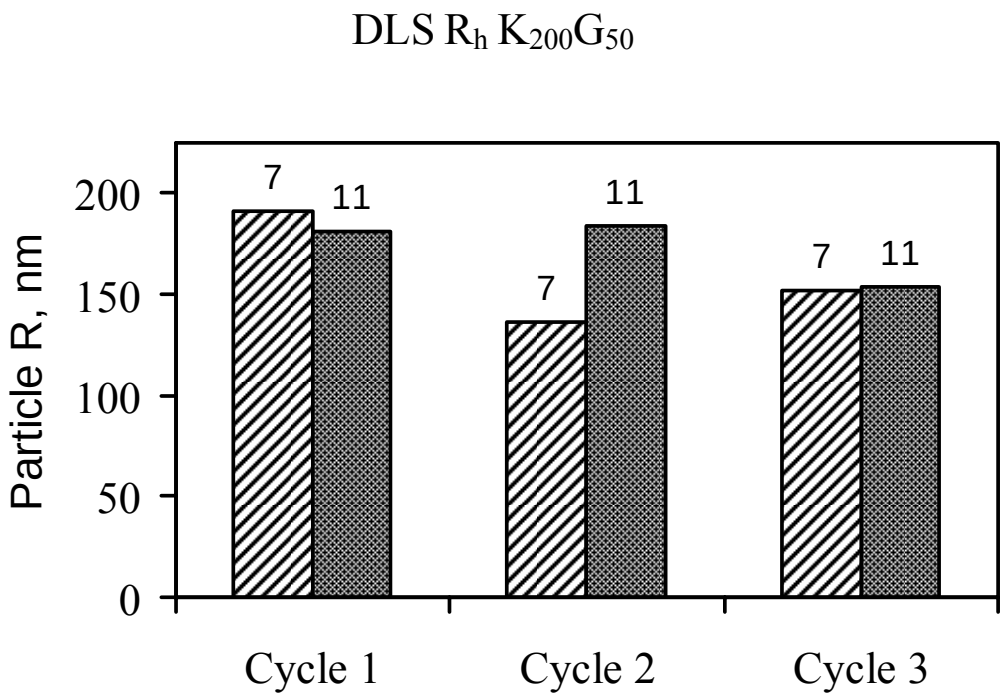

Figure IV-6: Results from a DLS pH swing. The same sample is used over the course of three cycles, starting out at pH 7, moving up to 11, then back down to 7, to start cycle 2.

For Figure IV-7, two different, but identically made, samples were tested. The two samples were a normally made vesicle solution, utilizing the normal vesicle formation procedure. The first sample was placed in a tube and tested, allowing the pH to rise and fall for two cycles. The second sample had the pH of the solution raised and lowered for two cycles before it was placed in a tube and tested. We see the same phenomenon happening with the SLS sample as we do with the DLS sample. Although the sizes are not exactly the same, we see the same general trend of the initial particle size being high, followed by the subsequent decrease in particles sizes for the following tests at pH 7. As the pH is raised and then lowered back to 7, we see the return to an average value for the particles in solution. DLS gave a value of 145 nm for the radius; SLS gives us around 137 nm for the radius.

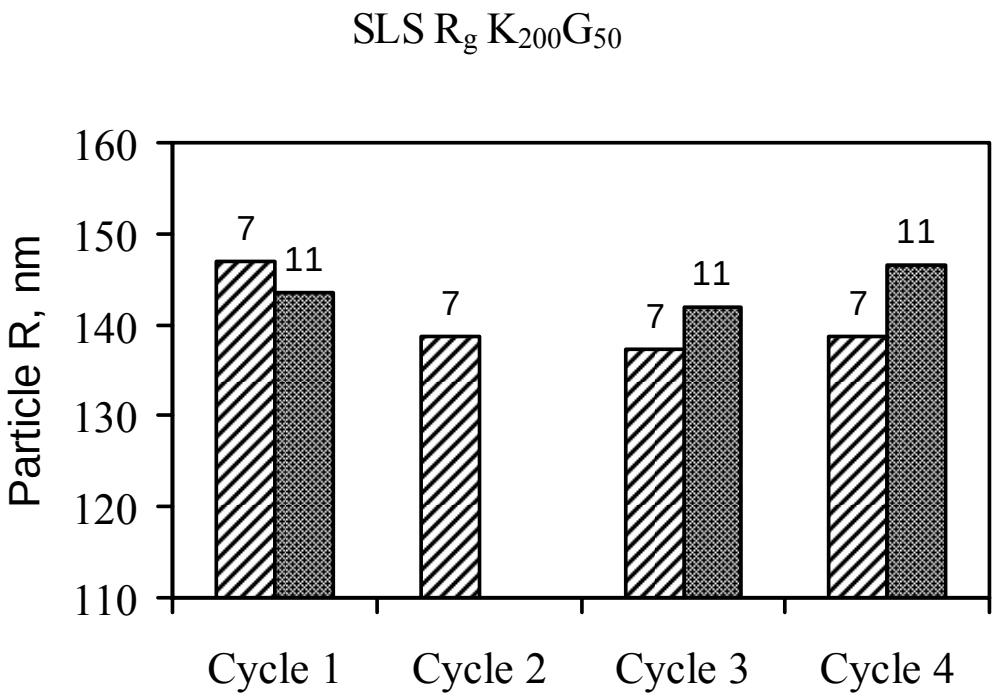

Figure IV-7: Results from a Guinier analysis on SLS data. Cycle 1 and 2 are the same sample; pH 11 for cycle 2 was not recorded. Cycle 3 and 4 are a different sample, raised up and down two times before the testing began. We see the particle radius for pH 7 come to a steady value, regardless of the cycle number.

4.4 Creation Methods

Another experiment was conducted to see how the particle size would vary depending on the creation method. This was done in part to make sure that the structures that are formed in solution are thermodynamically driven structures, as mentioned before, and not kinetically trapped aggregates. There were three overall samples: a dilution approach to making vesicles, and two normally made vesicle solutions, with one of the samples undergoing extrusion before being tested. The remaining normal vesicle solution was split in half, and one half of the solution underwent two pH swing cycles before being tested.

The overall results follow the same principles as the pH swing test. As the pH of the solution is increased, the polymer starts to aggregate in solution. This will give a non-reproducible number for the size of the particles at pH 11. Once the pH is returned to 7, we see size return to an average value for the samples.

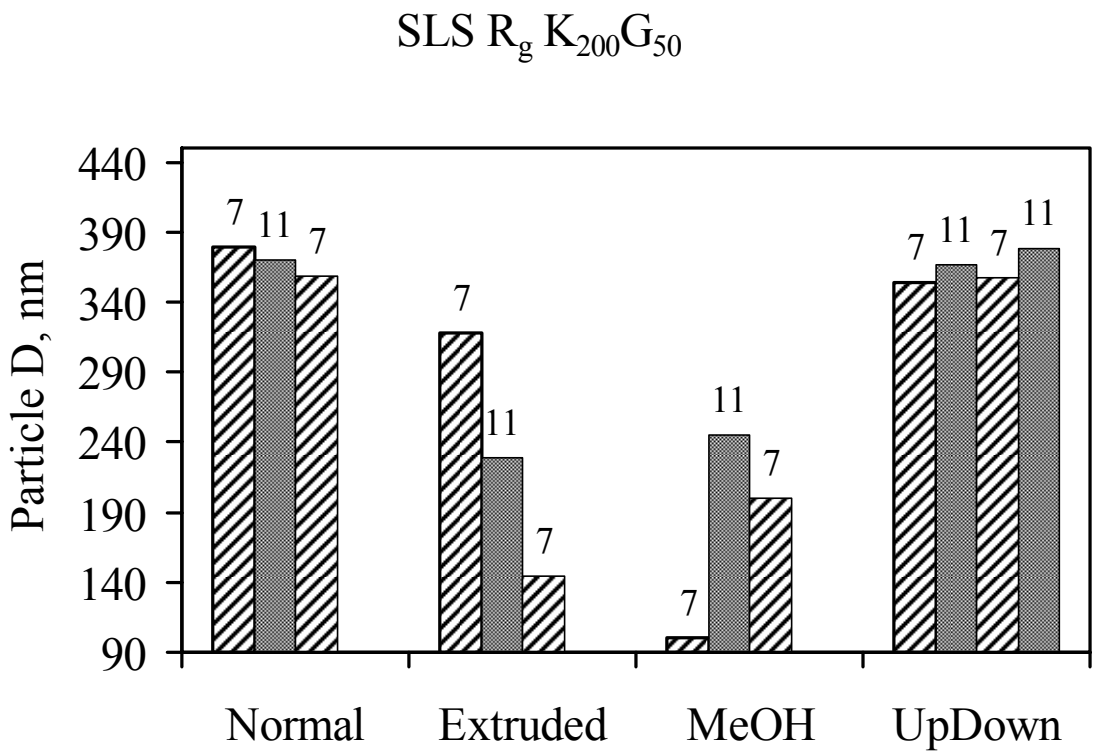

Figure IV-8: Results from the creation test. We have made vesicles using the polypeptide block copolymer utilizing various creation methods to prove that the particles in solution are thermodynamically driven to form vesicles, not kinetically trapped aggregates.

For the extruded sample, we notice that the particles start off smaller than the Normal or the UpDown, in part because the particles have been broken up and are more monodispersed than the other two samples. We see a drop in particle size for the vesicles when the pH is swung up and then back down, due to the fact that the particles are smaller to begin with.

With the Normal and UpDown samples, we see about the same response with the particle sizes as we saw with the other samples. We can see that the effect of increasing the pH and then decreasing does have an effect on the particle size, but not as dramatic as the change of pH on the extruded sample.

The MeOH sample offers the most interesting results. We have particles in solution at 100 nm in diameter, when the pH increases and then is brought back to pH 7, the size jumps up, to almost 200 nm. One explanation for this phenomenon is that when the polymer stock solution is transferred to the aqueous solution, the polymer chains, being dissolved monomerically, are not very close to each other. The structures formed in solution are very small vesicles, in part due to the dilute nature of the stock solution. When the pH is increased, the block copolymer chains collapse and aggregate, giving the polymer chances to aggregate into larger particles with the other polymer chains in solution. Once the pH is returned to pH 7, the chains can organize into a larger structure than before, due to the fact there are now more polymer chains close enough to each other to form a larger structure.

4.5 Vesicle Creation

These photos are the results of the experiment to see if the new polypeptide block copolymer would indeed form a self assembled bilayer. These photos were taken on the confocal microscope with Nile Red added to the film before the hydrating solution was added.

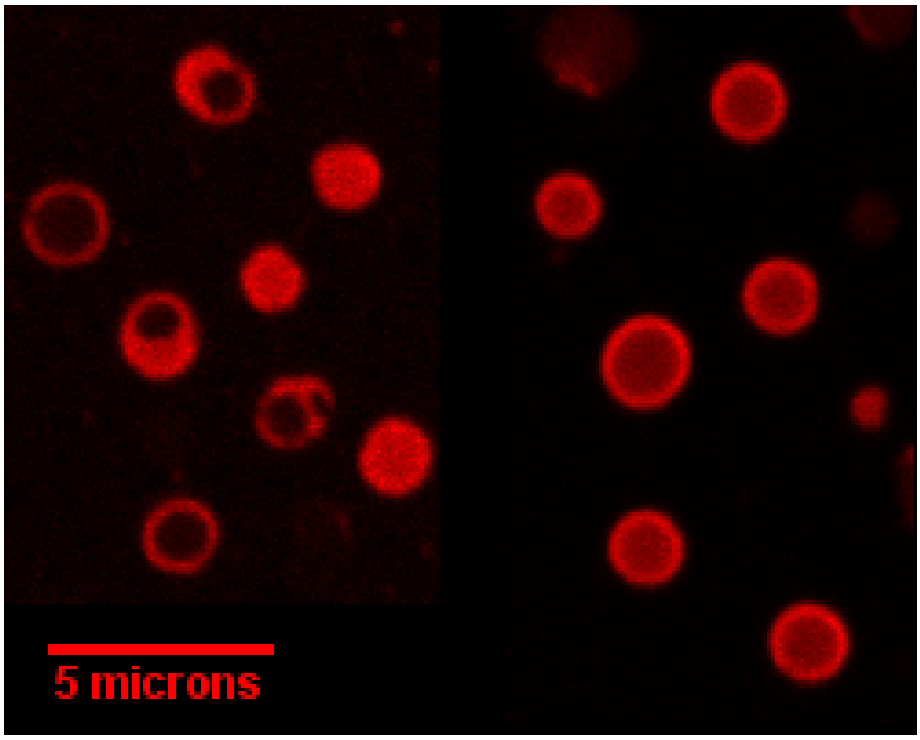

Figure IV-9: A field of view of vesicles around 2-3 microns. The vesicles show a definite bilayer region. The left and right panels are from the same sample, but different areas of the sample chamber.

The first issue with the novel polymer is to determine if the polymer is indeed creating vesicles. From the DLS and SLS studies, we know have particles in solution; determining what the structure was, either micelles or vesicles, required microscopy. Using the fluorescent bilayer method, Nile Red is incorporated into the bilayer of the polypeptide polymer. These samples are then imaged on the Leica confocal microscope. Figures IV-7 thru Figure IV-9 shows the results of the vesicles. Figure IV-9 shows small vesicles from the sample. We can see the halo of light indicative of a bilayer, with a small amount of light coming from the center of the ring. The photos were summed over a small range of individual photos, giving the figure. Regardless of the intensity of the center, a small annulus of the circle should be more intense than the rest of the circle.

From Figures IV-8 and Figure IV-9, we see the top and side profiles of two individual vesicles. Figure IV-10 has two large vesicles, around 10 microns. From the profile of the vesicles, we see the bilayer laying on the glass coverslip, with the top being a little out of focus, due to the Brownian motion affecting the top of the vesicle. Figure IV-11 shows the same phenomenon with a smaller vesicle, similar in size to Figure IV-10. These vesicles are only 2 microns in size, but exhibit the same characteristics of the larger vesicles.

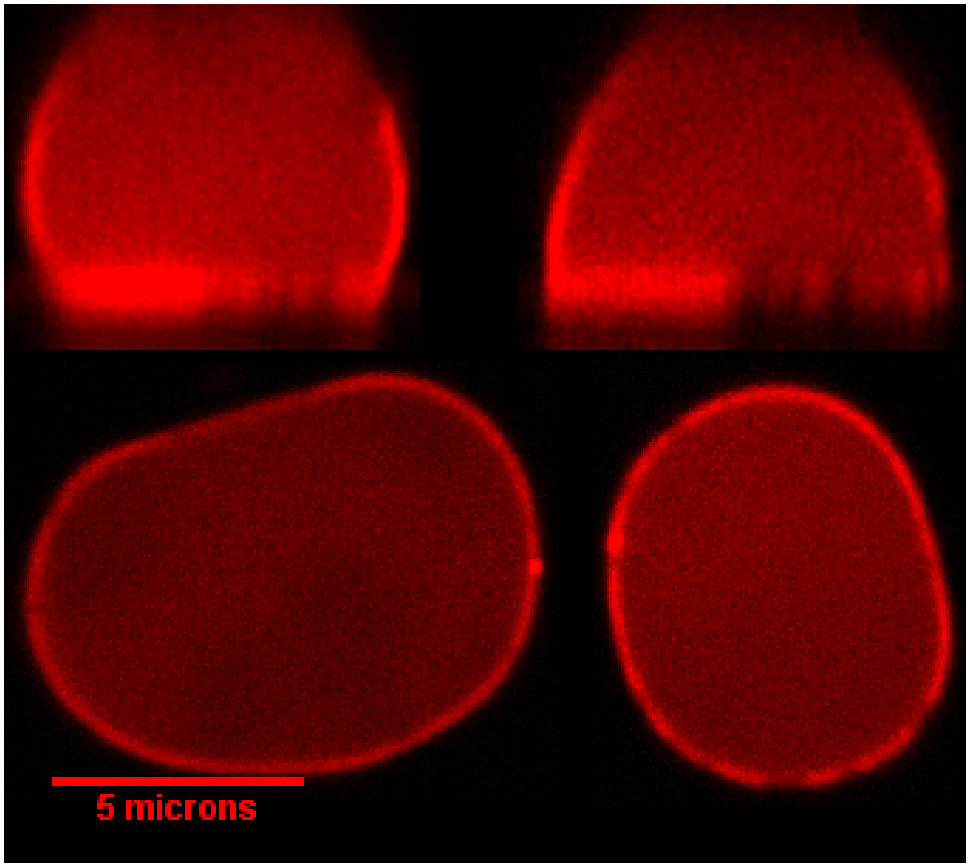

Figure IV-10: Large vesicles from the side. The left side is the same vesicle; the top left picture is an east to west view with the bottom left picture a top down view. The right side is the same vesicle; the upper right picture is a north south view, the bottom right picture is a top down view. Both vesicles are from the same sample, but different areas.

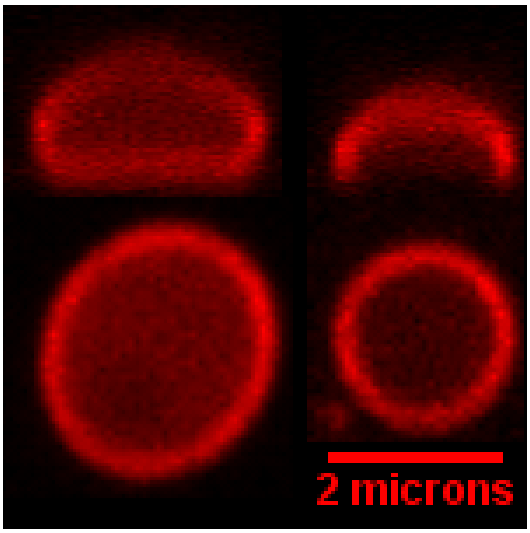

Figure IV-11: Smaller vesicles from the side. The left side is the same vesicle; the top left picture is an east to west view with the bottom left picture a top down view. The right side is the same vesicle; the upper right picture is a north south view, the bottom right picture is a top down view. Both vesicles are from the same sample, but different areas. The two vesicles are taken from the field of view picture.

V. FUTURE WORK AND CONCLUSIONS

5.1 Future Work with Encapsulation

5.1.1 New Monomer Systems

An avenue for future research is the encapsulation of various other polymers. The majority of the material characteristics study was done solely on acrylamide. The other two polymers mentioned in this paper, both NIPAM and PHEMA, have not been encapsulated and investigated. Also, other monomers need to be looked at to see if we can get true control of other, non-tested properties, such as density control. This can be as simple as testing other polymers, such as polyethylene oxide (PEG) or polylactic acid (PLA), or by changing either monomer concentration or crosslink density.

5.1.2 New Reaction Techniques

The polymerization technique in this set of experiments is solely based on radical polymerization. Using another polymerization technique, such as a condensation reaction, would open the way for other polymers to be encapsulated in vesicles. With condensation polymerization, an interpenetrating polymer network could be created. This could offer the ability to have a hard polymer as well as a hydrogel in the interior of a vesicle, offering a unique way of obtaining tunable material characteristics.

5.1.3 New Polymer Systems

Another experiment that is ongoing, but having some difficulties, due to the nature of the polymer, is encapsulating a monomer in the interior of a polypeptide block copolymer vesicle. Success has been achieved with other synthetic block copolymers used by the author in other experiments, but using the same approaches with the polypeptide block copolymer system has not been as successful. The main problem with encapsulating inside a polypeptide block copolymer vesicle is that the hydrophobic section cannot partition the interior as well as the synthetic block copolymers. Other approaches are needed to see if the monomer can be kept inside vesicle long enough to be trapped and then polymerized. This would allow the vesicle to possess an interior network while still maintaining a fluid bilayer.

5.1.4 Finite Element Analysis

A rigorous mathematical model to the material properties of the encapsulated microgels needs to be created. The vesicle system is a multi-component system when considering the mechanical response to different forces. The shell, internal polymer network and the bulk solution conditions all contribute to the amount of deformation the particle will undergo. We have independent measurements of the mechanical properties of each component that can be incorporated each into a numerical FEA to help elucidate where the majority of stress within the composite particle is concentrated. When we understand how particles with different structures distribute stress, we can use the numerical analysis to design specific mechanical properties for the biomimetic particles.

By creating a computer model, we should be able to model the expected behavior of particles in solution and predict the particle deformation to forces caused by solution conditions and adhesion.

5.2 Future Work with Polypeptide Block Copolymers

Future work for this polymer is quite extensive. Since this polymer is a novel polymer, little to no work has been done characterizing the material properties of the vesicles formed in solution. There are several types of block copolymers, differing in both ratios of the hydrophobic to hydrophilic blocks, as well as length of blocks. The polymers can be broken into two main categories, Lysine-Glysine blocks and Lysine-Alanine blocks. The blocks vary from a ratio of 2:1 to 4:1, with Lysine being the larger amount in both cases.

5.2.1 Material Properties

An experiment that would yield insight into the material properties of the vesicles would be micropipette aspiration to determine area expansion and bending modulus. Creating large vesicles and then aspirating the vesicles with a micropipette and then manipulating the vesicles to determine the moduli of the vesicles would be the first step in understanding this new polymer better. Pipette aspiration will follow similar studies using the synthetic block copolymers[73-75]. Since a wide range of polymers have been created, both the Lysine-Glysine blocks as well as the Alanine-Lysine blocks, we can

determine if the changing of the two block copolymers would have any affect on the material strength of the vesicle. Additionally, mixtures of both the Lysine-Glysine and Alanine-Lysine block copolymers will be investigated to see if the various material parameters can be modified due to changing the composition of the vesicles.

5.2.2 Phase Separation

Another project mentioned earlier is the phase diagram for the polypeptide polymer with a long chain hydrocarbon. There is some work going on trying to map out the phase behavior of several combinations of a synthetic block copolymer, $E_{89}Bd_{120}$, $E_{89}Bd_{120}$ with $K_{200}G_{50}$. By mapping out the phase behavior of the polypeptide polymer, we can possibly exploit this phenomenon through several avenues.

If the degree of phase separation can be determined from the previous experiment, then the next step would be to see if the phase separation could be controlled using a standard laboratory method, such as pH, temperature, or solution conditions. Following the conformational change of the polypeptide polymer due to pH, one approach would be to see if changing the pH of a mixed vesicle, one with synthetic block copolymers and polypeptides, if the polypeptide would change conformation without crashing out of the solution or vesicles. By doing this, we could get a concentration of polypeptide in one area, with an increased concentration of synthetic block copolymers in another area.

If one of the polymers has a particular chemical or compound of interest, this can lead to a site with an increased concentration of the compound. Before the vesicle was changed, the distribution of the compound could have been either too low to facilitate the

compound becoming active, or another compound prevents the interesting compound from activating. But by forcing the interesting compound to one area and the inhibitor to another, the compound can now become active.

5.2.3 Exterior Crosslinking

Another attempt at controlling phase separation would be to introduce light crosslinking with a pH sensitive crosslinker, such as disulfide bonds. If the two polymers do not want to evenly distribute throughout a vesicle, a vesicle could be formed through normal laboratory techniques then held into place with a crosslinker, the disulfide bond. If the vesicle is held to its current configuration, solution conditions could be changed, such as salt concentration or temperature, that would favor a particular state or shape. Since the vesicle is crosslinked, the change could not occur. Then when the particular change is desired, the pH is raised to break the crosslinks and the vesicle can change to relieve the stress. The pH can be lowered again and force the vesicle into a static state. The solution could then be changed back to the original state or another state, forcing the vesicle to want to change again, but is unable due to the crosslinking.

5.3 Conclusions

The results of these experiments show that we are able to create a cellular biomimic. We can create hollow vesicles ranging in size from 250 nm to 25 μm. The

size is confirmed by multiple experimental results: DLS, SLS, SEM and confocal imaging.

The second goal of creating a cellular mimic was the controllable surface chemistry. We have been able to develop a process to modify the current synthetic block copolymers, as well as being able to modify the polypeptide block copolymers already. We can attach any functional group to the end once the vesicles are created.

The third goal in creating a biomimic is being able to control the mechanical properties of the vesicle. We have shown that the interior of the vesicle can be made to offer similar mechanical abilities to natural systems.

The fourth goal is both having the fluid bilayer and a responsive particle to solution conditions. Due to the choice of polypeptide block copolymers, this comes built into the system. It has been shown that the vesicle forms a vesicle with a fluid bilayer as well as being responsive to solution conditions. The vesicle will exhibit different behavior in solutions in which the pH, as well as the salt concentrations, are modified.

REFERENCES AND NOTES

1. H.-A. Klok, S. Lecommandoux, *Advanced Polymer Science* **202**, 75 (2006).
2. G. M. Whitesides, J. P. Mathias, C. T. Seto, *Science* **254**, 1312 (Nov, 1991).
3. J. Babin, J. Rodriguez-Hernandez, S. Lecommandoux, H.-A. Klok, M.-F. Achard, *Faraday Discussions* **128**, 179 (2005).
4. F. Checot, S. Lecommandoux, H.-A. Klok, Y. Gnanou, *Eur. Phys. J. E* **10**, 25 (2003).
5. S. Fukushima, K. Miyata, N. Nishiyama, N. Kanayama, Y.Yamasaki, K.Kataoka,, *J. Am. Chem. Soc.* **127**, 2810 (2005).
6. A. Harada, K. Kataoka, *Macromolecules* **28**, 5294 (1995).
7. A. Harada, K. Kataoka, *Science* **283**, 65 (1999).
8. J. Rodrıguez-Hernandez, J. Babin, B. Zappone, S. Lecommandoux, *Biomacromolecules* **6**, 2213 (2005).
9. M. Yu, A. P. Nowak, T. J. Deming, D. J. Pochan, *J. Am. Chem. Soc.* **121**, 12210 (1999).
10. H. Bermudez, A. K. Brannan, D. A. Hammer, F. S. Bates, D. E. Discher, *Macromolecules* **35**, 8203 (2002).
11. H. Bermudez, D. A. Hammer, D. E. Discher, *Langmuir* **20**, 540 (2004).
12. B. M. Discher, D. A. Hammer, F. S. Bates, D. E. Discher, *Current Opinion in Colloid & Interface Science* **5**, 125 (2000).
13. B. M. Discher, Y.Won, D. Ege, J. Lee, F. Bates *et al.*, *Science* **284**, 1143 (May, 1999).

14. D. E. Discher, Eisenberg, A, *Science* **297**, 967 (2002).

15. D. A. Hammer, D. E. Discher, *Annu. Rev. Mater. Res.* **31**, 387 (2001).

16. B. M. Discher, H. Bermudez, D. Hammer, D. Discher, Y. Won *et al.*, *J. Phys. Chem. B* **106**, 2848 (2002).

17. J. J. Lin, J. Silas, H. Bermudez, V. Milam, F. Bates *et al.*, *Langmuir* **20**, 5493 (2004).

18. J. N. Israelachvili, D. J. Mitchell, B. W. Ninham, *Biochim. Biophys. Acta* **470**, 185 (1977).

19. P. Attard, D. J. Mitchell, B. W. Ninham, *Biophysical Journal* **53**, 457 (1988).

20. M. Bostrom, V. Deniz, B. W. Ninham, *J. Phys. Chem. B* **110**, 9645 (2006).

21. J. J. Lin, P. P. Ghoroghchian, Y. Zhang, D. A. Hammer, *Langmuir* **22**, 3975 (2006).

22. J. J. Lin, F. S. Bates, D. A. Hammer, J. A. Silas, *Physical Review Letters* **95**, 026101 (2005).

23. S. K. Bhatia, D. A. Hammer, *Langmuir* **18**, 5881 (2002).

24. C. E. Orsello, D. A. Lauffenburger, D. A. Hammer, *Trends in Biotechnology* **19**, 310 (2001).

25. H.-P. Hentze, E. W. Kaler, *Current Opinion in Colloid and Interface Science* **8**, 164 (2003).

26. M. Antonietti, C. Goltner, H.-P. Hentze, *Langmuir* **14**, 2670 (1998).

27. H. P. Hentze, E. Kramer, B. Berton, S. Forster, M. Antonietti *et al.*, *Macromolecules* **32**, 5803 (1999).

28. M. Jung, D. Hubert, P. Bomans, P. Frederik, J. Meuldijk *et al.*, *Langmuir* **13**, 6877 (1997).

29. J. Hotz, W. Meier, *Advanced Materials* **10**, 1387 (1998).

30. S. Mann, S. Burkett, S. Davis, C. Fowler, N. Mendelson *et al.*, *Chem. Mater.* **9**, 2300 (1997).

31. D. H. W. Hubert, M. Jung, A. German, *Advanced Materials* **12**, 210 (2000).

32. D. H. W. Hubert, M. Jung, A. L. German, *Advanced Materials* **12**, 1291 (2000).

33. S. Forster, B. Berton, H. P. Hentze, E. Kramer, M. Antonietti *et al.*, *Macromolecules* **34**, 4610 (2001).

34. M. Muthukumar, C. K. Ober, E. L. Thomas, *Science* **277**, 1225 (1997).

35. G. M. Whitesides, J. P. Mathias, C. T. Seto, *Science* **254**, 1312 (1991).

36. S. C. Glotzer, M. J. Soloman, N. A. Kotov, *AIChE Journal* **50**, 2978 (2004).

37. B. P. Binks, S. O. Lumsdun, *Phys. Chem. Chem. Phys.* **1**, 3007 (1999).

38. D. B. Lawrence, T. Cai, Z. Hu, M. Marquez, A. D. Dinsmore, *Langmuir* **23**, 395 (2007).

39. H. Deng, D. L. Gin, R. C. Smith, *J. Am. Chem. Soc.* **120**, 3522 (1998).

40. O. Lade, C. C. Co, P. Cotts, R. Strey, E. W. Kaler, *Colloid Polym. Sci.* **283**, 905 (2005).

41. M. Jung, I. Ouden, A. Montoya-Goni, D. H. W. Hubert, P. Frederik *et al.*, *Langmuir* **16**, 4185 (2000).

42. W. Meier, J. Hotz, *Langmuir* **14**, 1031 (1998).

43. C. A. McKelvey, E. W. Kaler, *Journal of Colloid and Interface Science* **245**, 68 (2002).

44. C. A. McKelvey, E. W. Kaler, J. A. Zasadzinski, B. Coldren, H.-T. Jung, *Langmuir* **16**, 8285 (2000).

45. A. Graff, M. Winterhalter, W. Meier, *Langmuir* **17**, 919 (2001).

46. A. Jesorka, M. Markstrom, O. Orwar, *Langmuir* **21**, 1230 (2005).

47. T. J. Deming, *Nature* **390**, 386 (1997).

48. A. P. Nowak, V. Breedveld, L. Pakstis, B. Ozbas, D. Pine *et al.*, *Nature* **417**, 424 (2002).

49. E. G. Bellomo, M. D. Wyrsta, L. Pakstis, D. J. Pochan, T. J. Deming, *Nature Materials* **3**, 244 (2004).

50. E. P. Holowka, D. J. Pochan, T. J. Deming, *J. Am. Chem. Soc.* **127**, 12423 (2005).

51. E. A. Minich, A. P. Nowak, T. J. Deming, D. J. Pochan, *Polymer* **45**, 1951 (2004).

52. D. J. Pochan, L. Pakstis, B. Ozbas, A. P. Nowak, T. J. Deming, *Macromolecules* **35**, 5358 (2002).

53. F. Checot, J. Rodrıguez-Hernandez, Y. Gnanou, S. Lecommandoux, *Biomolecular Engineering* **24**, 81 (2007).

54. F. Checot, A. Brulet, J. Oberdisse, Y. Gnanou, O. Mondain-Monval *et al.*, *Langmuir* **21**, 4308 (2005).

55. V. Breedveld, A. P. Nowak, J. Sato, T. J. Deming, D. J. Pine, *Macromolecules* **37**, 3943 (2004).

56. T. J. Deming, *J. Am. Chem. Soc.* **120**, 4240 (1998).

57. T. J. Deming, S. A. Curtin, *J. Am. Chem. Soc.* **122**, 5710 (2000).

58. L. Pakstis *et al.*, *Biomacromolecules* **5**, 312 (2004).

59. D. F. DeTar, R. Silversteid, *J. Am. Chem. Soc.* **88**, 1013 (1966).

60. D. F. DeTar, R. Silverstein, *J. Am. Chem. Soc.* **88**, 1020 (1966).

61. D. R. Halpin, J. A. Lee, S. J. Wrenn, P. B. Harbury, *PLOS BIOLOGY* **2**, 1031 (2004).

62. M. M. Rozenman, D. R. Liu, *ChemBioChem* **7**, 253 (2006).

63. A. Guinier, G. Fournet, *Small-Angle Scattering of X-Rays* (John Wiley and Sons, New York, 1955).

64. J. William D. Callister, *Material Science and Engineering* (John Wiley & Sons, New York, 2003).

65. K. K. Liu, D. R. Williams, B. J. Briscoe, *J. Phys. D: Appl. Phys.* **31**, 294 (1998).

66. M. E. R. Shanahan, *J. Adhesion* **63**, 15 (1997).

67. J. N. Israelachvili, *Intermolecular & Surface Forces* (Academic Press, New York, 1992).

68. A. V. Kyrylyuk, J. G. E. M. Fraaije, *Journal of Chemical Physics* **121**, 2806 (2004).

69. N. Dan, M. Tirrell, *Macromolecules* **26**, 4310 (1993).

70. A. V. Kyrylyuk, J. G. E. M. Fraaije, *Journal of Chemical Physics* **121**, 9166 (2004).

71. A. S. Lee, M. Santore, F. Bates, D. Discher, *Macromolecules* **35**, 8540 (2002).

72. S. Forster, N. Hermsdorf, C. Bottcher, P. Lindner, *Macromolecules* **35**, 4096 (2002).

73. E. Evans, D. J. Klingenberg, W. Rawicz, F. Szoka, *Langmuir* **12**, 3031 (1996).

74. D. H. Kim, A. L. Klibanov, D. Needham, *Langmuir* **16**, 2808 (2000).

75. J. C.-M. Lee, M. Santore, F. S. Bates, D. E. Discher, *Macromolecules* **35**, 323 (2002).

APPENDIX

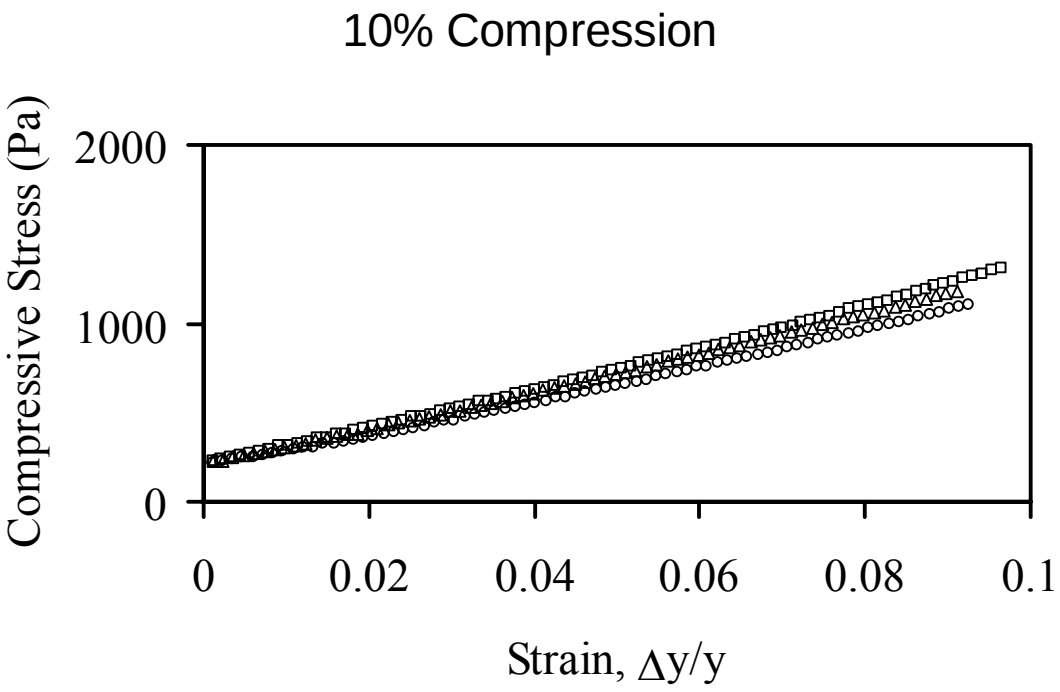

Figure A-1: The 19:1 5% AM compression test. The first graph is the 10% compression test. The middle graph is the 20% compression test, and the bottom graph is the 40% failure compression test. The values from the graphs are tabulated in Table III-3. The open circle (○) is the first cylinder, the open square (□) is the second cylinder and the open triangle (Δ) is the third cylinder.

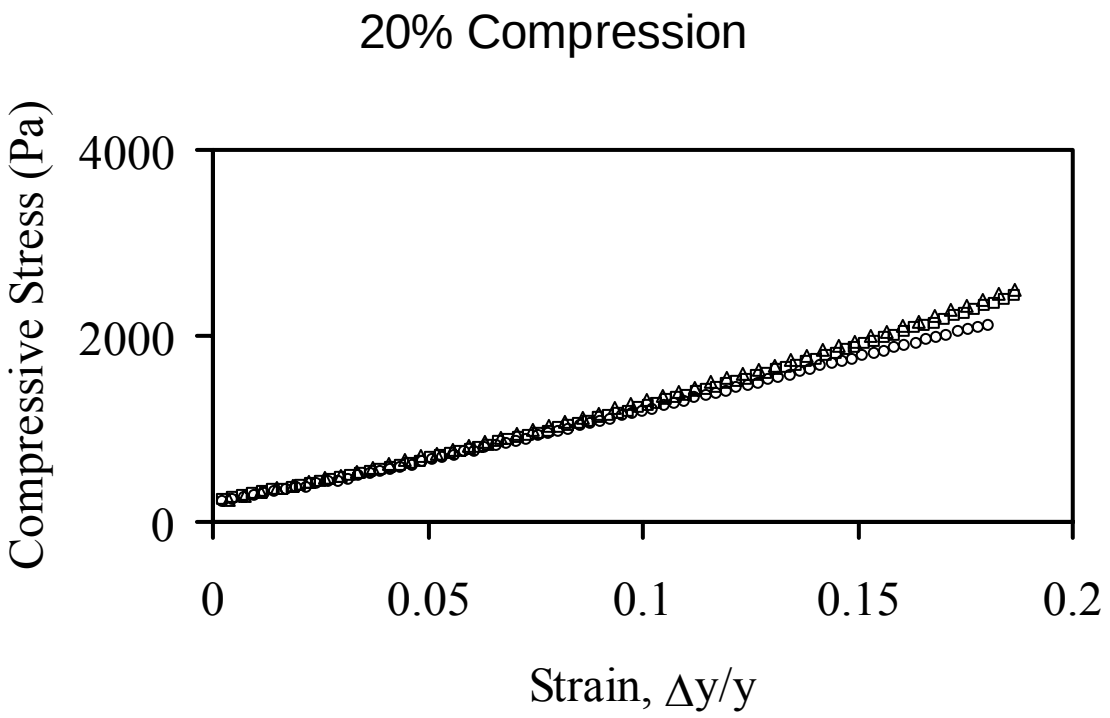

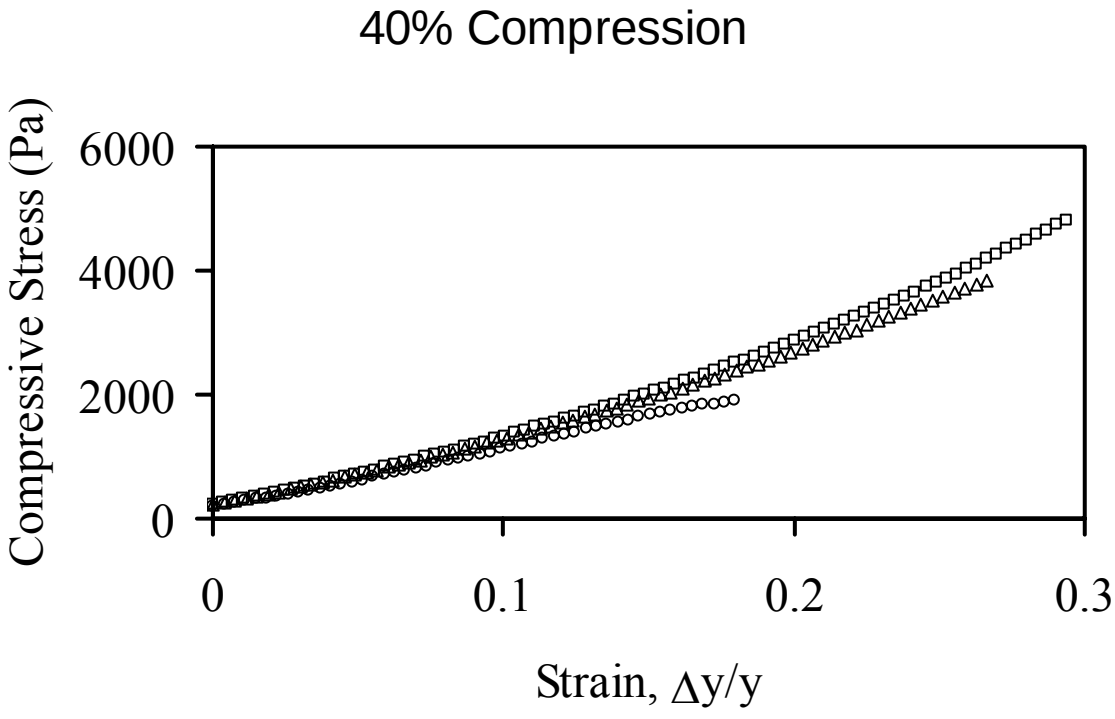

Figure A-1 continued.

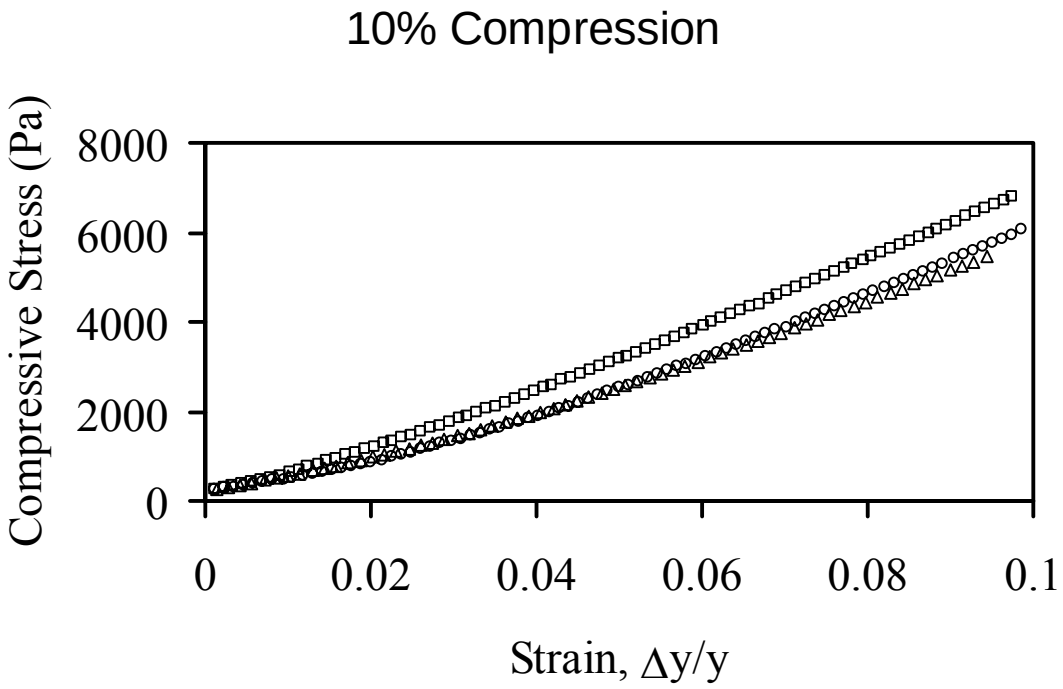

Figure A-2: The 19:1 10% AM compression test. The first graph is the 10% compression test. The middle graph is the 20% compression test, and the bottom graph is the 40% failure compression test. The values from the graphs are tabulated in Table III-3. The open circle (○) is the first cylinder, the open square (□) is the second cylinder and the open triangle (Δ) is the third cylinder.

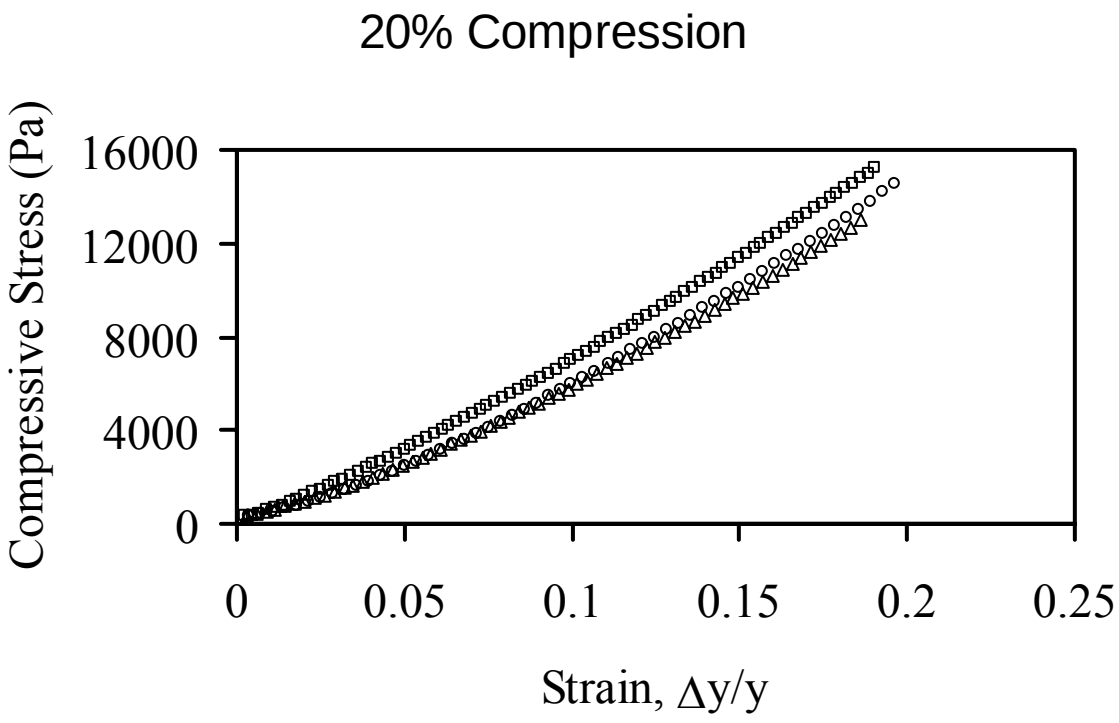

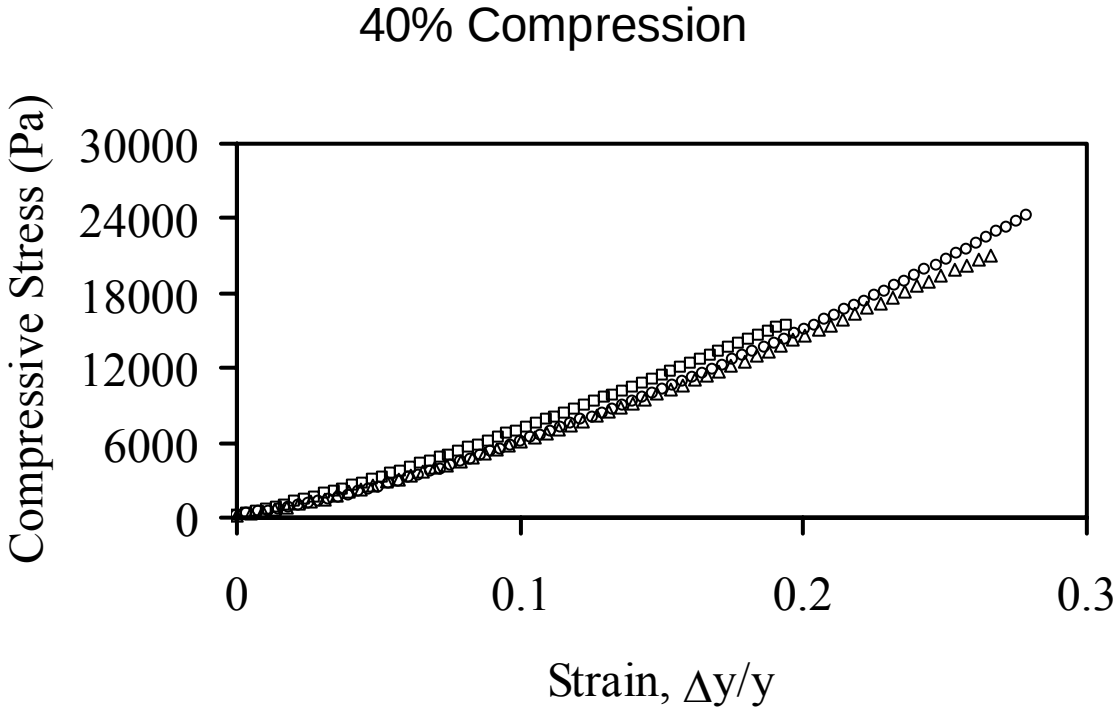

Figure A-2 continued.

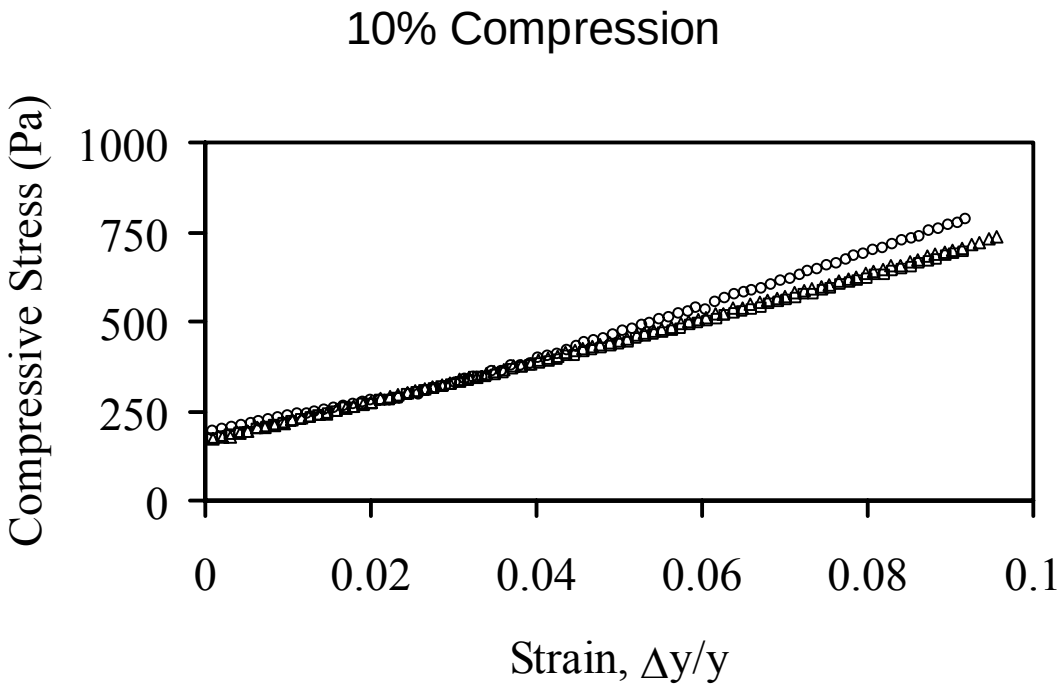

Figure A-3: The 38:1 5% AM compression test. The first graph is the 10% compression test. The middle graph is the 20% compression test, and the bottom graph is the 40% failure compression test. The values from the graphs are tabulated in Table III-4. The open circle (○) is the first cylinder, the open square (□) is the second cylinder and the open triangle (Δ) is the third cylinder.

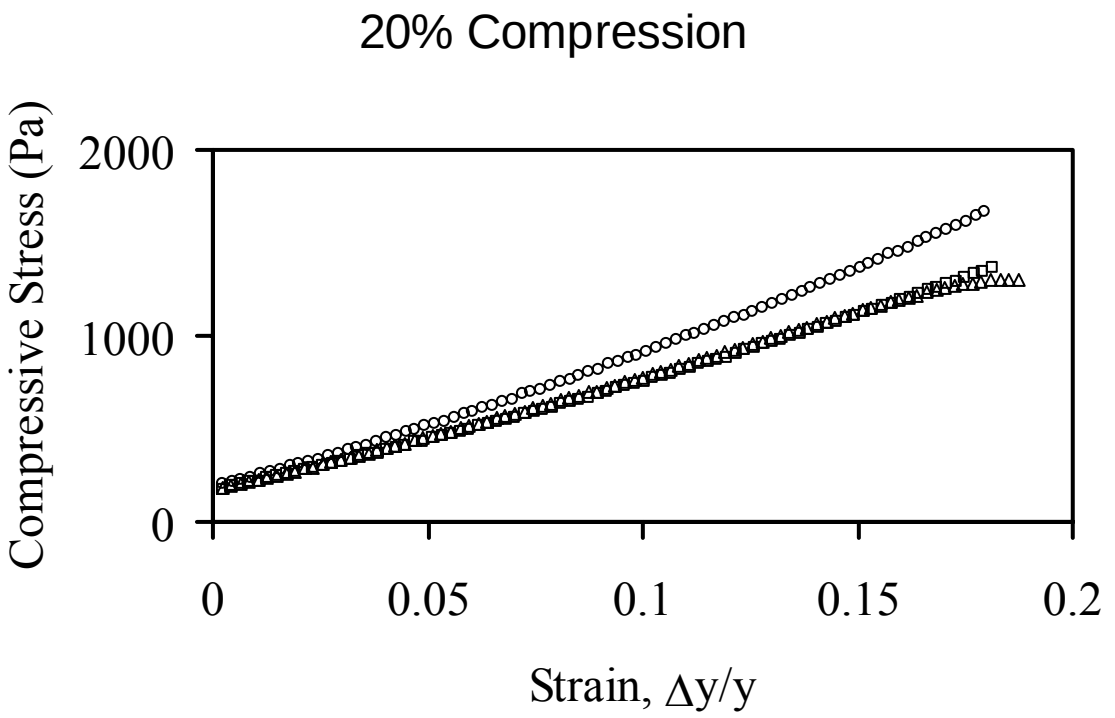

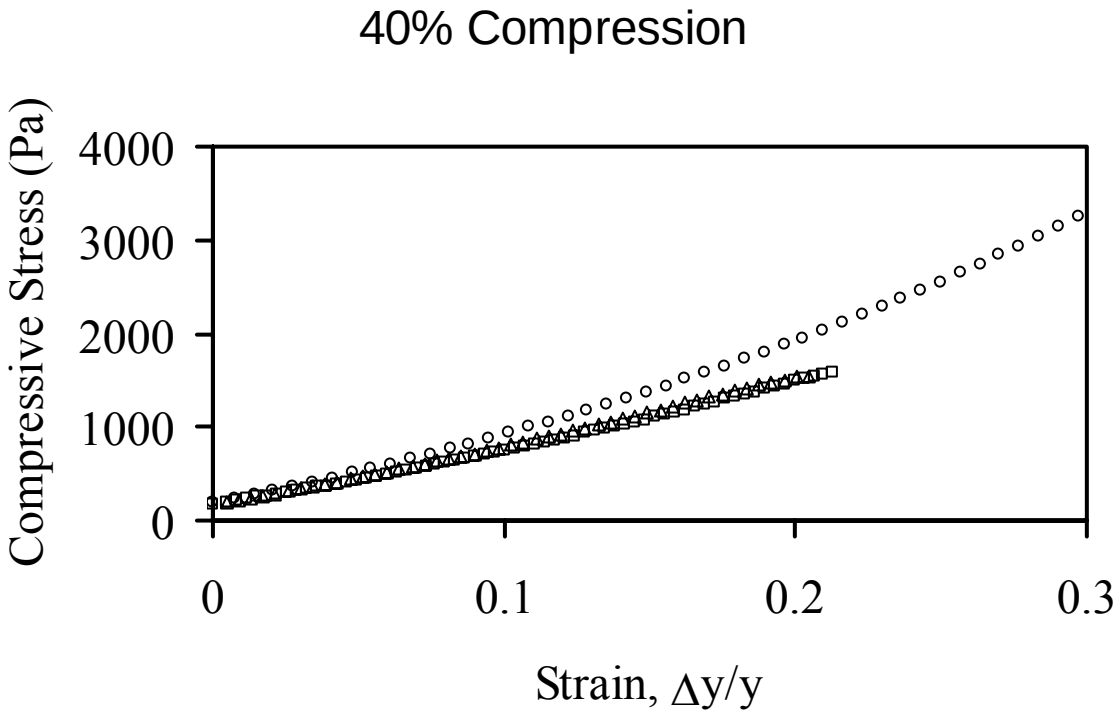

Figure A-3 continued.

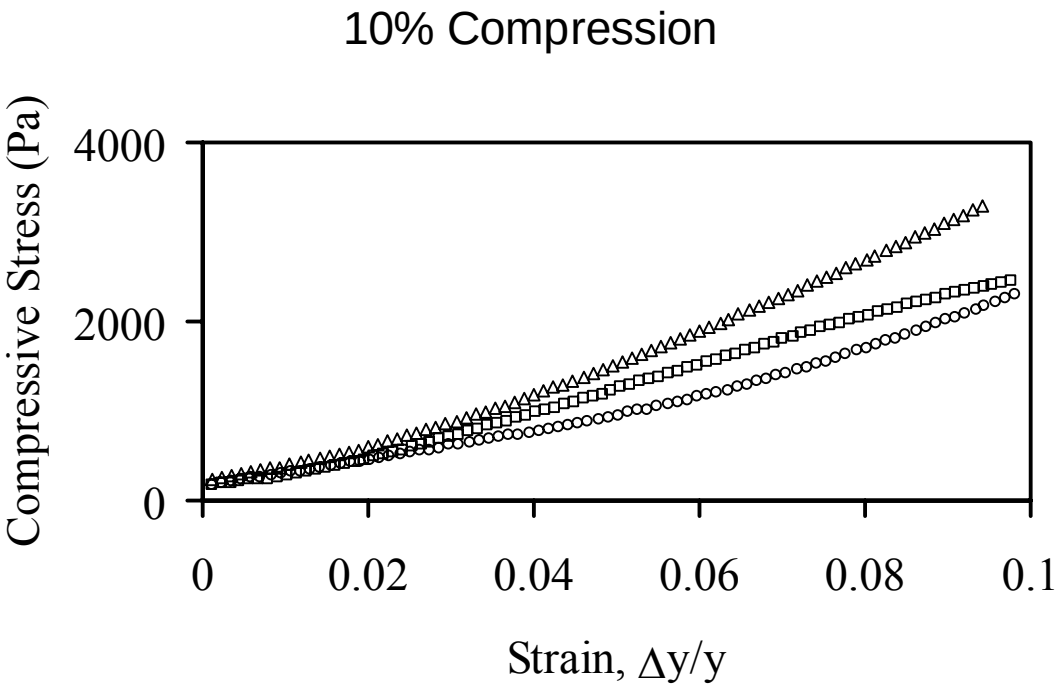

Figure A-4: The 38:1 10% AM compression test. The first graph is the 10% compression test. The middle graph is the 20% compression test, and the bottom graph is the 40% failure compression test. The values from the graphs are tabulated in Table III-4. The open circle (○) is the first cylinder, the open square (□) is the second cylinder and the open triangle (Δ) is the third cylinder.

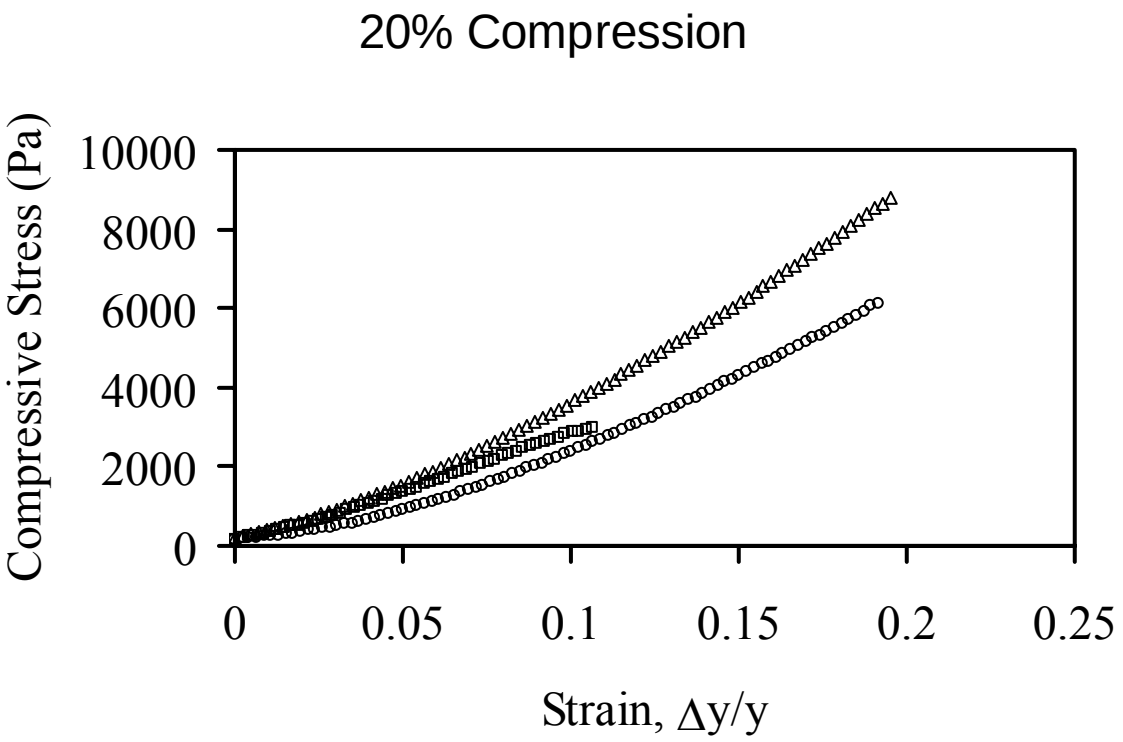

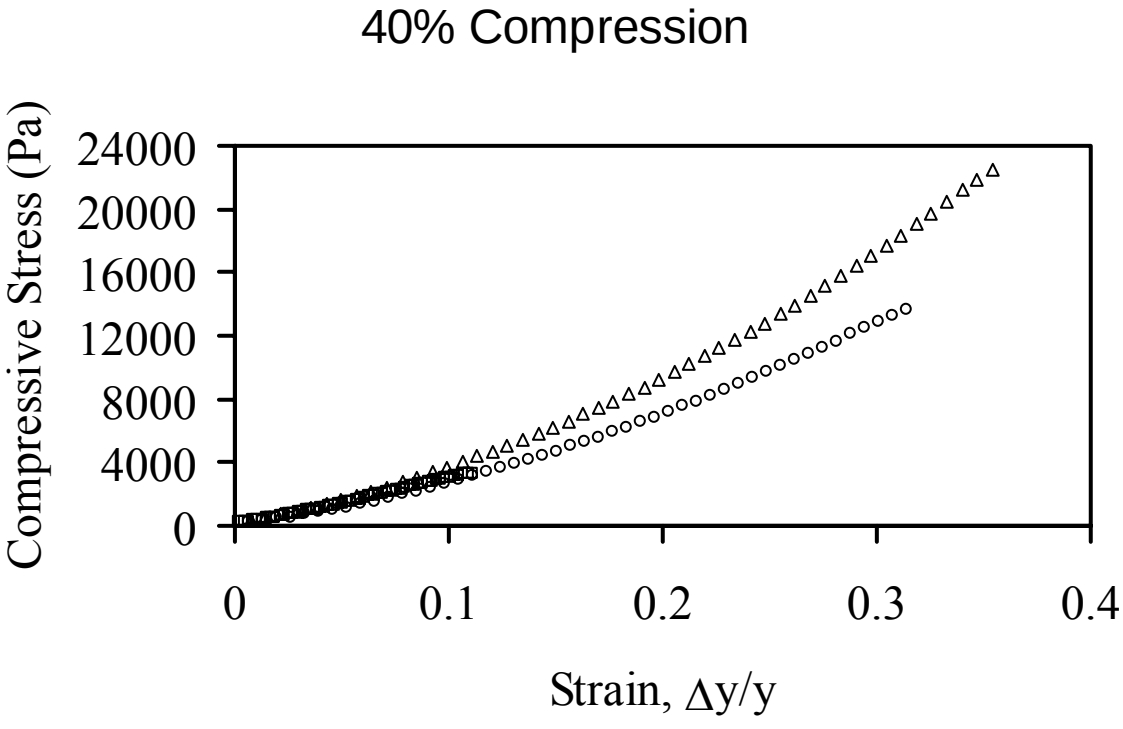

Figure A-4 continued.

VITA

Name:	Jeffery Simon Gaspard
Address:	PO Box 8336
	College Station, TX 77840
Email address:	jsg@tamu.edu
Education:	B.S., Chemical Engineering, Texas A&M University, 2005
	M.S., Chemical Engineering, Texas A&M University, 2007